Received: 30 June 2018 | Revised: 29 October 2018 | Accepted: 29 October 2018
DOI: 10.1002/gj.3397

RESEARCH ARTICLE

WILEY

Geochemical characteristics of igneous rocks associated with Baghu gold deposit in the Neotethyan Torud-Chah Shirin segment, Northern Iran

Shojaeddin Niroomand[1] | David R. Lentz[2] | Fatemeh Sepidbar[1] | Hossein Ali Tajeddin[3] | Jamshid Hassanzadeh[4] | Hassan Mirnejad[1]

[1] School of Geology, College of Science, University of Tehran, Tehran, Iran

[2] Department of Earth Sciences, University of New Brunswick, Fredericton, New Brunswick, Canada

[3] Department of Geology, Faculty of Basic Sciences, Tarbiat Modarres University, Tehran, Iran

[4] Division of Geological and Planetary Sciences, California Institute of Technology, Pasadena, California

Correspondence
Shojaeddin Niroomand, School of Geology, College of Science, University of Tehran, Tehran 1417614411, Iran.
Email: niroomand@ut.ac.ir

Funding information
NSERC Discovery

Handling Editor: I. Somerville

The Baghu gold deposit, hosted by a granitoid stock as well as volcanic rocks, is located in Northern Iran. The igneous rocks consist of granodiorite and granite as well as volcanic rocks, such as basaltic andesite and andesite, which are cut by dioritic dykes. The igneous rocks have metaluminous, high K calc-alkaline, and island-arc signatures, characterized by enrichment in large-ion lithophile elements (LILEs) and depletion in high-field-strength elements (HFSEs). Zircon separates yield U–Pb ages of 47, 43, and 38 Ma for the volcanics, granitoid rocks, and dyke, respectively, indicating that the magmatism associated with gold–copper mineralization occurred during the Eocene. The low Ba/Th, Th/Nb, Ba/La, and Th/Yb ratios in igneous rocks indicate that their mantle source was not likely modified by subduction activity. A comparison of La/Sm against La (ppm), similar Th/Nb and Th/Yb, and average $(La/Yb)_n$ ratios to the crust and lower continental crust (LCC) suggests that the magmatism in the Baghu was likely associated with partial melting of juvenile lower crust, induced by north-westward subduction of the Neo-Tethys oceanic lithosphere in an extensional setting.

KEYWORDS

Baghu gold deposit, geochemistry, island arc, lower continental crust, partial melting, zircon U–Pb age

1 | INTRODUCTION

Cenozoic magmatic rocks cover much of Iran to the north of the Zagros suture zone (Figure 1). Although their ages vary from Palaeocene to Quaternary, the Eocene pulse is more predominant (Asiabanha, Bardintzeff, Kananian, & Rahimi, 2012; Verdel, Wernicke, Hassanzadeh, & Guest, 2011). Three Cenozoic magmatic arcs are recognized in Iran (Figure 1) including (i) the Alborz magmatic arc in east–west direction, which continues into the magmatic belts of Pontides in Turkey (Castro, Aghazadeh, Badrzadeh, & Chichorro, 2013; Dilek, Imamverdiyev, & Altunkaynak, 2010); (ii) the Urumieh–Dokhtar Magmatic Arc (UDMA), formed by north-eastward subduction of the Neotethyan Ocean beneath Iran (Berberian & King, 1981); and (iii) the east Iranian magmatic arc, formed as the result of eastward subduction of the Birjand-Sistan Ocean beneath the Lut Block. These Cenozoic igneous rocks are separated by ophiolitic suture zones of Zagros, Sabzevar, and Birjand-Sistan (Figure 1).

Available data from the Frontal arc of UDMA show that Cenozoic magmatic pulses have occurred from ~54 Ma to 37 Ma, although recent studies also suppose a younger magmatic pulse at 20–5 Ma (Aghazadeh, Hou, Badrzadeh, & Zhou, 2015; Asadi, Moore, & Zarasvandi, 2014; Chiu et al., 2013). Decompression melting of lithospheric mantle hydrated by the Neo-Tethys slab-derived fluids and post-collisional convective removal of thickened subcontinental mantle lithosphere has been proposed for the Frontal arc magmatism during the Cenozoic time (Aghazadeh et al., 2015; Asadi et al., 2014). To the north and north-east of the Frontal arc system of the UDMA, extensive outer arc basins including

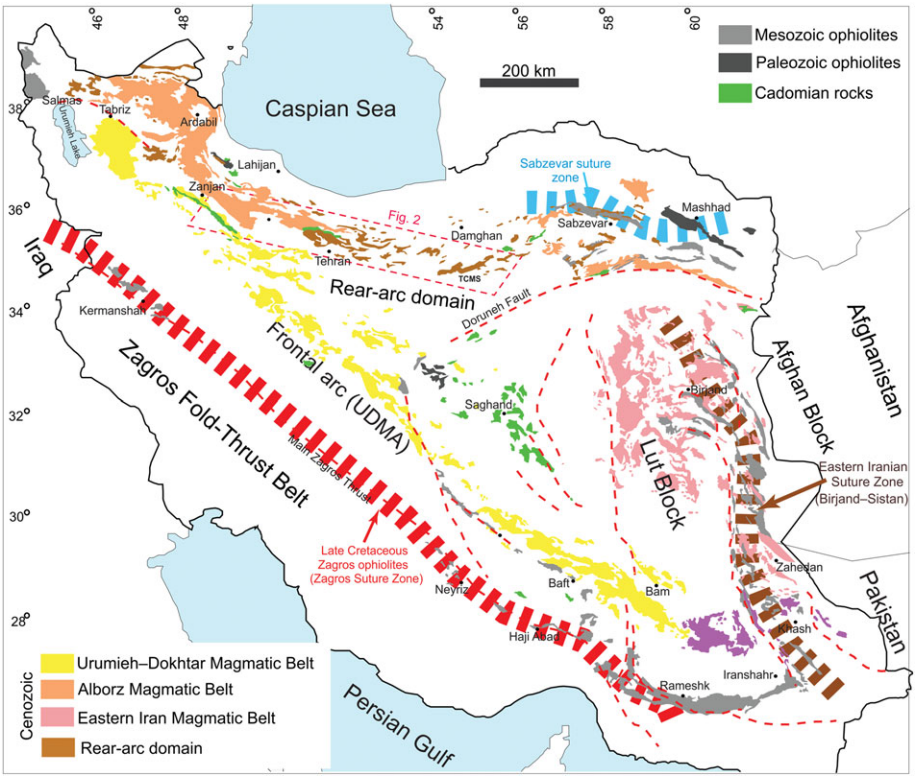

FIGURE 1 Map of Iran showing location of Baghu gold deposit (in the Torud-Chah Shirin Magmatic Segment, TCMS) (Modified after Shafaii Moghadam and Stern, 2014). [Colour figure can be viewed at wileyonlinelibrary.com]

the Torud-Chah Shirin magmatic segment (TCMS) developed during the latest Cretaceous to Eocene. However, the magmatism in the rear-arc domain, in Northern Iran between Zanjan and Damghan, is still relatively unexplored, and different scenarios have been suggested, including the expansion of an outer arc or an extensional rear arc. Baumann, Spies, and Lensch (1983) determined the initial $(^{87}Sr/^{86}Sr)_i$ ratios of the young volcanic rocks (0.7035–0.7055) within the Sabzevar–Quchan–Kashmar magmatic sector in the east of TCMS and suggested that the parental magma of such rocks was generated by the dehydration of an oceanic crust and by the partial melting of the mantle wedge above a subduction zone. The Eocene TCMS hosts many small mineral occurrences to particularly base- and precious metal-bearing veins such as Baghu (Au ± Cu), Darestan (Au–Cu), Gandy (Au–Ag–Pb–Zn), Abolhassani (Pb–Zn–Ag–Au), Cheshmeh Hafez (Pb–Zn), Chalu (Cu), Chahmessi (Cu), Pousideh (Cu), Pb–Zn, Reshm (Pb–Zn), Khanjar (Pb–Zn), and Anaru (Pb–Zn) (Fard, Rastad, & Ghaderi, 2006; Moradi, 2010; Niroomand, Hassanzadeh, & Tajeddin, & Asadi, 2018; Rastad, Fard, Rashidnejad-Omran, & Ghaderi, 1999; Shamanian, Hedenquist, Hattor, & Hassanzadeh, 2004; Shaykhi, 2013) and Bavanat (Pb–Zn–Cu–Au) (Asadi et al., 2014; Asadi & Moore, 2017).

In this study, we present a new dataset of geochemical and geochronological (zircon U–Pb) analysis for the magmatic rocks of the Baghu gold deposit (Niroomand et al., 2018) in the rear-arc domain. The main aims of this paper are to find the timing of the arc magmatism in rear-arc region, magma types and sources, and magmatic and tectonic regime as they relate to the fundamental controls on mineralization.

2 | GEOLOGY

The rear-arc region is formed in response to the progressive thinning of the continental crust associated with an extensional setting during Cenozoic time in Iran. It was formed by large magmatism generating up to ~3,000-m-thick volcanic sequences and pyroclastic edifices along with sedimentary intercalations (Figure 2). Considerable intrusive bodies that range in composition from gabbro to granite are also present in the rear-arc region. Based on the new age information, the rear-arc Cenozoic magmatism was continuous from ~49 to 36 Ma (early to late Eocene). The Eocene TCMS that is 10–12 km wide and 100–110 km long and strikes NE–SW from Torud to Chah Shirin is known as part of the Eocene rear-arc magmatism through the north of Iran. The TCMS comprises metamorphic rocks of Precambrian age covered by Palaeozoic epicontinental sedimentary rocks. Peak magmatic activity occurred from middle to possibly late Eocene and has been divided into three stages, from the oldest to the youngest (Houshmandzadeh, Alavi Naini, & Haghipour, 1978) including (1) explosive volcanic activity represented by rhyolitic to rhyodacitic tuffs and locally andesitic lava flows, with subordinate marls, tuffaceous marlstones, and sandstones; (2) lava flows and pyroclastic rocks of andesite, trachyandesite, and basaltic andesite composition; and (3) subordinate dacitic-rhyodacitic rocks and hypabyssal intrusive rocks. Structural patterns are controlled by two principal strike–slip faults, Anjillo in the north and Torud in the south, both with north-east trends. The Baghu gold deposit is located within the TCMS and consists dominantly of Eocene intermediate to acidic lava flows of basaltic andesite, andesite, trachyandesite, and dacite; and volcanic breccias

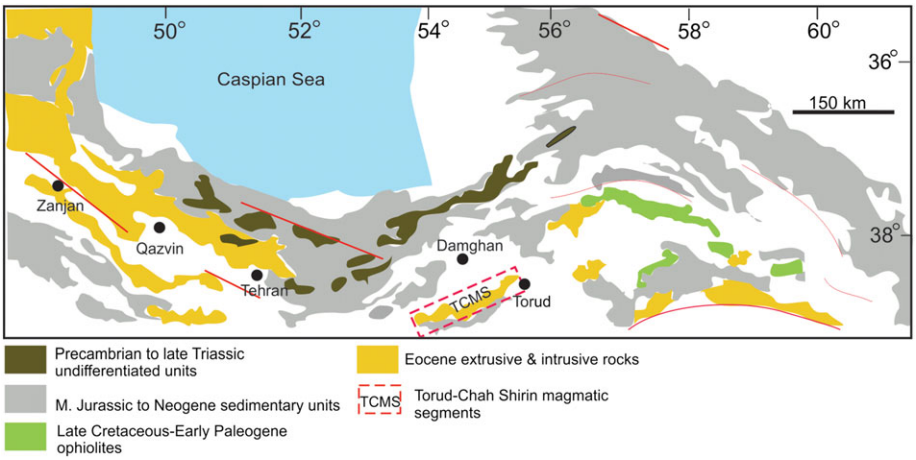

FIGURE 2 Northern part of geological Map of Iran, showing rear-arc domain and associated units (modified after Zanchi et al., 2009) (and location of TCMS) [Colour figure can be viewed at wileyonlinelibrary.com]

and subvolcanic intrusions, such as micro-quartz diorite, quartz monzodiorite, micro-granodiorite, and micro-granite, which are cut by several dykes (Figure 3). The main host rocks for the gold deposit are the micro-granodiorite and micro-granite.

The local stratigraphy has been subdivided into four units, from the oldest to the youngest:

1. A sequence of thin-bedded green to purple tuffs with trachydacite and dacite composition, and massive grey tuff breccia with dacite to dacitic andesite composition.
2. Intermediate lava flows of andesite and trachyandesite.
3. Grey to green tuffs, volcanic breccias, and intermediate lava flows with andesitic to dacitic composition of middle Eocene age.
4. Subvolcanic crypto domes, hypabyssal plutons, and several dykes intruded the above volcanic sequence during the middle to upper Eocene. These bodies caused a wide range of hydrothermal alteration assemblages in the Baghu region.

3 | REGIONAL GEOLOGY, SAMPLE DESCRIPTION, AND PETROGRAPHY

The Baghu igneous rocks at the north of the Lut Block are the northward continuation of the UDMA. They include volcanic and plutonic rocks, which are cut by dykes. The Baghu volcanic rocks occupy an area of about 5 km^2 and occur as a lava dome, which is surrounded and intruded by different fault systems (Figure 3). The volcanic rocks in Baghu are dominantly andesite and basalt in composition, and their contact with Eocene granitoids is obvious in the eastern parts, whereas in the western parts, the volcanic rocks are tectonically juxtaposed with Quaternary alluvium and fluidal deposits (Figure 3). In the TCMS, the rock units are situated between two major faults, the Torud Fault to the south and Anjillo Fault in the north. These units consist of highly fractured rock in this fault zone that served as the conduit for the hydrothermal fluid. Hydrothermal alteration and mineralization at the Baghu gold deposit are centred on the hypabyssal granodiorites

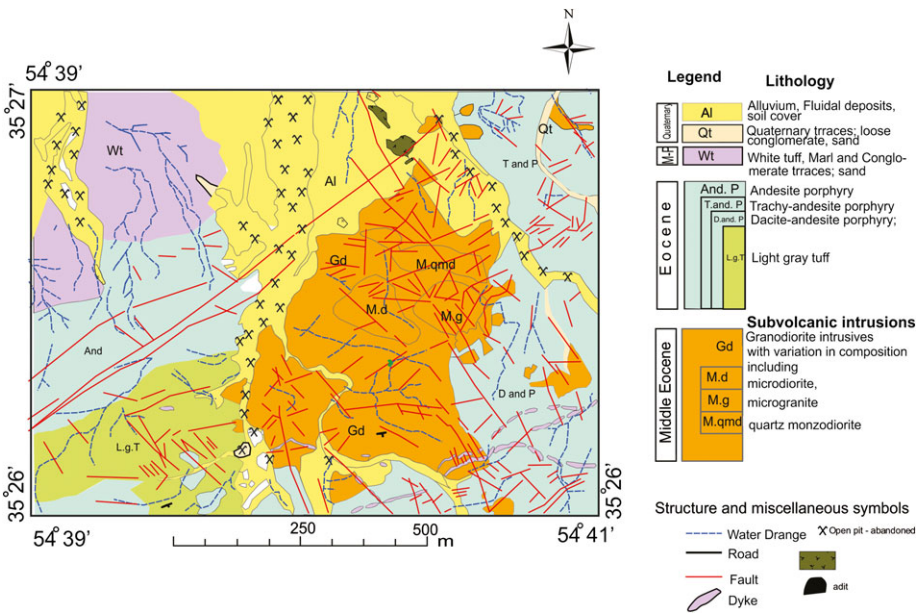

FIGURE 3 Geological map of the Baghu deposit (modified after Rashidnejad-Omran, 1992) [Colour figure can be viewed at wileyonlinelibrary.com]

Colour online, B&W in print

and micro-granites (Figure 4a–e). Field observations and petrologic studies in the Baghu deposit area show that the typical alteration zones consist of propylitic, phyllic, sericitic, chloritic, argillic, advanced argillic, and silicic assemblages. The unique association of tourmaline and turquoise is an eminent feature of this deposit. The peripheral propylitic alteration at the Baghu deposit is characterized by formation of montmorillonite, chlorite, epidote calcite, quartz, and pyrite (Figure 4a,b). The supergene alteration is significant in the Baghu area. Kaolinite and iron oxy-hydroxides are widespread (Figure 4c) and have replaced up to 50% of the hypogene sulphide minerals. Malachite, azurite, covellite, digenite, and chalcocite are also present. Hydrothermal tourmaline typically occurs as disseminations, aggregates, pods, and veins within the intrusive rocks or as alteration envelopes and veins along pluton contacts and in the Eocene volcanic country rocks associated with the widespread phyllic alteration (Figure 4d,e). The Baghu tourmaline (Figure 4d,e) is a dravite-schorl solid solution, with an almost dravite end-member composition (Taghipour & Mackizadeh, 2014).

The Baghu andesites are characterized by locally vesicular structure and porphyritic, granular, glomero-porphyritic, trachytic, vesicular, and amygdaloidal textures. The main rock-forming minerals are euhedral to subhedral phenocrysts of plagioclase (~40%), clinopyroxene (~10%), amphibole and biotite (~5%), and quartz (less than 2%) (Figure 5a–d). Magnetite and apatite are found as accessory mineral (less than 3%). Subhedral to anhedral plagioclase (0.5–2 mm) shows alteration to kaolinite and sericite. Plagioclases are lath-shaped, zoned crystals, and their composition is generally andesine. Coarse-grained plagioclase is characterized by disequilibrium dusty and/or sieve textures (Figure 5a–d). Clinopyroxenes are lath-shaped and zoned. Quartz is rare and occurs as an interstitial phase between plagioclase and clinopyroxene. The basalts are known by locally vesicular structure and ophitic, subophitic, porphyritic, glomero-porphyritic, and vesicular textures. The main rock-forming minerals are euhedral to subhedral phenocrysts of plagioclase (~35%) and clinopyroxene (~15%). Magnetite is found as accessory mineral (less than 3%). Plagioclases are lath-shaped, zoned crystals, and their composition is generally labradorite. Coarse-grained plagioclase is characterized by disequilibrium dusty and/or sieve textures. Similar to andesite, clinopyroxenes are lath-shaped and zoned.

Granitoids are exposed as stocks in the central part of the Baghu gold deposit (Figure 3). Field observations show that the Eocene granitoids crosscut Cenozoic volcanic and pyroclastic rocks. Granitoids are

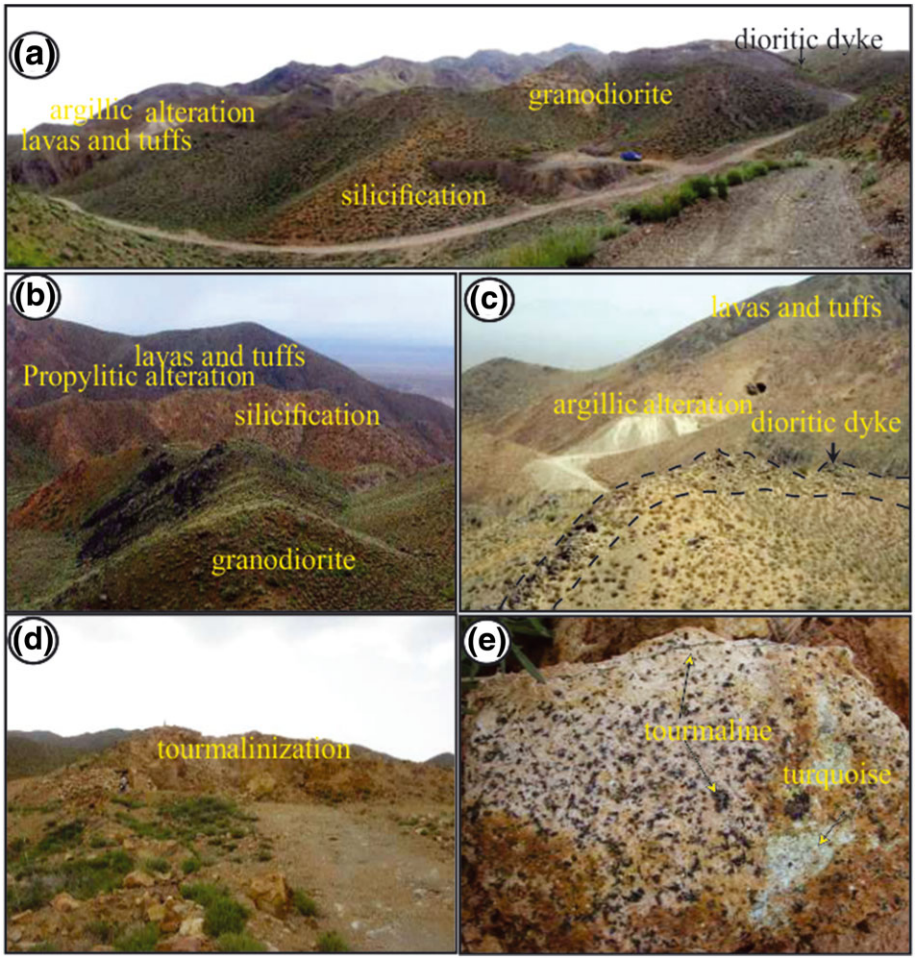

FIGURE 4 (a) Photographs of the rock units and hydrothermal alterations in Baghu gold deposit, looking south to southwest. (b) Hydrothermal alteration: Silicification has rendered these hills resistant to erosion. Lavas exposed in the green hill and subvolcanic intrusions show creamy to brown on the photo. (c) Post-Eocene diorite dyke cut the Middle–Upper Eocene lavas and tuffs succession. (d) Outcrop of tourmaline alteration overprinting microdiorite intrusion. (e) Intense tourmaline alteration overgrowing diorite rock as a disseminated and veinlets [Colour figure can be viewed at wileyonlinelibrary.com]

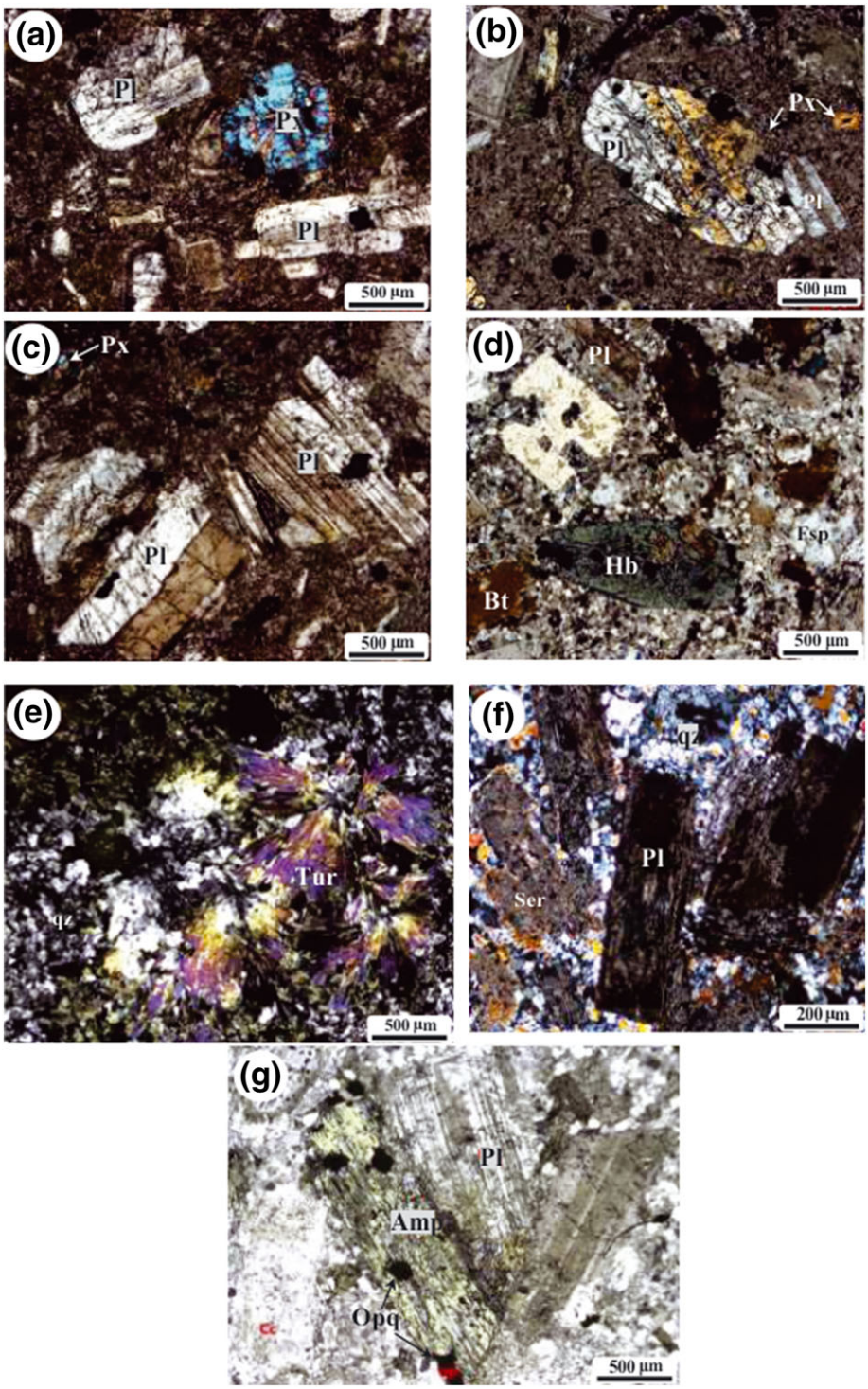

FIGURE 5 Photomicrographs illustrating the mineralogy and textures of rocks in the Baghu area, XPL. (a, b) Porphyry texture with plagioclase and pyroxene phenocrysts in andesite-basalt. (c) Plagioclase phenocrysts with polysynthetic and Carlsbad twins in andesite. (d) Hornblende and biotite crystals in micro-granite. (e) Intense tourmaline alteration in micro-granite. (f) Sericitized plagioclase phenocrysts in mineralized micro-granite. (g) Chloritized amphibole in granodiorite. Amp, amphibole; Bt, biotite; Chl, chlorite; Hbl, hornblende; Opq, opaque mineral; Pl, plagioclase; Px, pyroxene; Fsp, feldspar; Ser, sericite; Tur, Tourmaline, Tqz, tourquoise; abbreviations after Whitney and Evans (2010) [Colour figure can be viewed at wileyonlinelibrary.com]

Colour online, B&W in print

subdivided into micro-quartz diorite, quartz monzodiorite, micro-granodiorite, and micro-granite, which are all cut by several dioritic dykes. Granodiorites, the host rocks for the gold deposit in the Baghu area, are abundant and extensive in the central part of Baghu gold deposit and exhibit granular to micro-granular and micro-porphyritic textures. Petrographically, these rocks show a variety of textures, which are mostly micro-granular with a lesser occurrence of grano-phyric and porphyritic textures. Granodiorites have abundant euhedral to subhedral phenocrysts of plagioclase (40–42%), quartz (25–30%), K-feldspar (22–24%), amphibole, and/or biotite (4–5%) (Figure 5g). Subhedral to anhedral K-feldspar (0.5–2 mm) is usually perthitic. Quartz occurs in two generations: as euhedral, early-formed crystals

and anhedral late-stage grains. Magnetite, ilmenite, zircon, apatite, and titanite are the principal accessory phases. The extensive association of tourmaline and turquoise is an eminent feature of this granitoid (Figure 5e,f).

The granodioritic body in some parts crops out as a micro-granite, which is dominated by quartz, plagioclase, alkali feldspar, and biotite with accessory titanite, zircon, and apatite. Plagioclase is present as laths, often with Carlsbad twins, and is partly replaced by sericite.

The other intrusive bodies in the southern portion of the village of Baghu range from monzodiorite to quartz monzodiorite. The colour of monzodioritic rocks changes from grey, due to loss of mafic minerals, to green, due to the addition of epidote. The minerals are medium size with a micro-granular to micro-porphyritic texture under the microscope. Granophyric, porphyry, and trachytic textures are also observed. The main minerals include plagioclase, amphibole, and quartz, whereas the minor minerals are made up of biotite, apatite, titanite, and opaque minerals. Chlorite, epidote, sericite, titanite, and clay minerals are the alteration products.

The small outcrops of dioritic rocks in the study area mainly contain plagioclase, clinopyroxene, and amphibole. Apatite, tourmaline, titanite, and opaque minerals constitute the accessory minerals, while chlorite, muscovite, epidote, sericite, and clay minerals making up the secondary minerals. The textures range from granular to micro-granular, micro-porphyritic, ophitic, and intersertal. Plagioclases occur as subhedral to euhedral crystals.

4 | SAMPLING AND ANALYTICAL METHODS

This study includes eight whole-rock analyses from different intrusive units and eight analyses from volcanic rocks and three analyses from dykes. Whole-rock major and trace element concentrations were measured by X-ray fluorescence (XRF) and inductively coupled plasma–mass spectrometry (ICP–MS) in China (Table 1). The ICP–MS analyses were carried out after sample digestion using an HF–HNO_3 mixture in high-pressure Teflon bombs. Pure Rh solution was used as an internal standard to monitor the drift, and reference materials were Chinese national rock standards (BHVO-2, AGV-2, G2, G3, and GSR-3). Details of analytical procedures can be found in Qi, Hu and Gregoire (2000). The precision and accuracy of the ICP–MS analyses are estimated to be better than approximately 5% for most trace elements.

To establish the age of the igneous rock from the Baghu gold deposit, we have analysed three samples for zircon U–Pb ages including granitoids (granodiorite), volcanic rocks (andesite), and dyke. Zircon separates were obtained from 6 to 7 kg of crushed rock samples by handpicking under a binocular microscope after sieving and then applying conventional heavy liquid and magnetic separation techniques at the Geological Survey of Iran. The zircon U–Pb ages are based on U, Pb, and Th isotopic measurements employing spot analyses using the Cameca IMS 1270 ion microprobe at the University of California, Los Angeles. Analytical methods follow the procedures described by Quidelleur et al. (1997) and Schmitt et al. (2003). Following mineral separation using conventional liquid and magnetic techniques, zircon grains were hand-selected, mounted in epoxy, and coated with ~100 Å of gold. The ion-microprobe spot analyses utilized a primary ion beam focused to a ~30-μm-diameter spot and a secondary ion beam with a mass resolving power of 5,000 and energy window of 50 eV. Following a pre-sputtering period of ~180 s, each analysis collected data for 8–10 cycles. The sample chamber was flooded with oxygen at ~3×10^{-5} Torr to enhance secondary Pb^+ ionization. The reported weighted mean ages are based on $^{206}Pb/^{238}U$ ages calculated using zircon standard AS3 (1,099 ± 0.5 Ma; Paces & Miller, 1993). Common lead corrections were made using the measured values of ^{204}Pb (Stacey & Kramers, 1975) and the values of ^{208}Pb corrected for ^{232}Th-derived ^{208}Pb (Compston, Williams, & Meyer, 1984), which are considered a proxy for common ^{206}Pb and ^{207}Pb. These corrections use the anthropogenic Pb compositions reported for the Los Angeles basin (Sanudo-Wilhelmy & Flegal, 1994).

5 | RESULTS

5.1 | Geochemistry

Whole-rock chemical compositions of representative samples from Baghu are given in Table 1. In the total alkalis vs. silica diagram of Middlemost (1994), most of the Baghu plutonic rocks plot in the granodiorite and granite fields (Figure 6a). The volcanic rocks and dykes fall in the fields of subalkaline basalt, andesite, and andesite-basalt in the Zr/TiO_2 versus Nb/Y classification diagram of Winchester and Floyd (1977) (Figure 6b). Granitoids are characterized by higher contents of SiO_2 (63.9–74.3 wt.%), Al_2O_3 (7.8–14.1 wt.%), and K_2O (2.5–6.7 wt.%) and low K_2O/Na_2O ratios (0.7–1.3; except two samples that show high K_2O/Na_2O ratios of 8.2 and 14.6) relative to volcanic rocks, whereas volcanic rocks and dykes have low contents of SiO_2 (48.5–58.5 wt.%), K_2O (2.02–3.5 wt.%), moderate-to-high content of Al_2O_3 (13.3–19.5 wt.%), MgO (1.5–5.9 wt.%), and FeO (5.5–12.5 wt.%). In the $Al_2O_3/(CaO + K_2O + Na_2O)$,i.e., A/CNK, versus SiO_2 diagram (Shand, 1974), the granitoids and volcanic rocks as well as dykes mostly plot into the metaluminous domain (Figure 6c). Based on $K_2O–SiO_2$ (Figure 6d) diagram, the intrusive rocks have typically calc-alkaline to shoshonitic signatures, in agreement with volcanic rocks and dykes (Figure 6d). In the Rb/Zr vs. Nb diagram (Brown, Thorpe, & Webb, 1984), Cenozoic Baghu magmatic rocks lie within the island-arc field (Figure 6e). They are characterized by high Sr (300–958 ppm) and low Y (4.5–29.9 ppm) and Yb (0.9–2.5 ppm) contents. The low-to-moderate ratios of Sr/Y (20.05–76.6) of the Baghu plutonic as well as volcanic rocks resemble those of normal arc rocks, except one sample of granitoids with high ratio of 118 (Figure 6f).

Chondrite-normalized (Sun & McDonough, 1989) rare earth element (REE) patterns for the Baghu plutonic rocks show enrichment in light REEs (LREEs) relative to heavy REEs (HREEs) ($(La/Yb)_n$ = 4.2–8.2), without negative Eu anomalies (Figure 7a). In a primitive mantle-normalized (Sun & McDonough, 1989) multi-element diagram, enrichment in Rb, Ba, Th, U, and K and negative anomalies in Nb and Ti are conspicuous (Figure 7b). Similar to granitoids, volcanic rocks and dykes show enrichment in LREEs, LILEs compared to HREEs ($(La/Yb)_n$ = 6.4–22.2) and HFSEs, without negative Eu anomalies (Figure 7c,f).

TABLE 1 Whole-rock major and trace element concentrations (ppm) of the Baghu igneous rocks

	Sample number																		
	BA31	BA32	BA33	BA34	BA35	BA37	BA38	BA39	BA40	BA42	BA45	BA46	BA47	BA48	BA49	BA50	BA51	BA52	BA53
SiO_2	55.5	48.5	49.83	54.51	54.47	57.1	58.02	58.5	63.9	72.3	72.2	74.3	68.4	65.1	65.7	72	56 63	54.02	56.02
TiO_2	0.78	0.1	0.66	0.51	0.51	0.49	0.49	0.9	0.52	0.38	0.24	0.4	0.38	0.71	0.58	0.26	0.7	0.88	0.83
Al_2O_3	17.07	17.74	16.44	15.3	15.43	15.89	17.5	13.33	14.04	11.31	12.42	7.8	12.97	11.9	13.44	12.17	19.48	16.69	14.69
MnO	0.21	0.03	0.15	0.11	0.11	0.11	0.11	0.13	0.06	0.06	0.01	0.05	0.03	0.17	0.01	0.03	0.12	0.14	0.11
MgO	3.15	4.49	5.78	5.96	5.95	3.93	3.03	3.35	2.17	1.32	0.89	1.41	1.61	3.05	2.26	0.66	1.57	3.76	3.76
CaO	5.43	7.32	8.15	6.22	6.78	6.61	5.89	6.52	1.86	2.2	0.18	1.67	2.16	3.76	4.45	0.4	6	7.59	6.95
Na_2O	4.1	3	4.58	4.76	4.51	3.72	4.73	3.59	4.73	2.91	0.82	3.42	3.21	3.9	3.36	0.29	4.24	3.19	4.91
K_2O	2.63	2.8	2.41	3.63	3.31	2.89	2.02	2.02	5.22	3.66	6.72	3.91	4.08	2.82	2.57	4.17	3.47	2.88	3.18
P_2O_5	0.35	0.49	0.36	0.29	0.29	0.28	0.22	0.43	0.23	0.19	0.58	0.21	0.22	0.44	0.48	0.14	0.46	0.33	0.23
Fe_2O_3 T	8.38	12.45	8.4	6.82	6.85	6.5	5.86	8.18	5.54	3.24	3.26	3.91	4.03	5.96	4.27	7.49	5.56	8.36	6.36
LOI	2.25	2.55	2.06	0.88	0.92	1.54	1.01	2.55	2.55	2.55	2.55	2.55	2.55	2.55	2.55	2.35	1.28	1.4	1.4
Total	99.85	99.46	98.82	98.99	99.13	99.06	98 87	99.51	100.82	100.13	99.86	99.63	99.64	100.34	99.67	99.96	99.51	99 24	99 24
Cs	2.65	3.03	1.9	2.6	1.8	2.4	2.65	1.99	2.6	1.85	3.32	2.98	1.95	2.03	1.61	2.67	1.32	1.79	1.49
Rb	70.88	64.05	30.08	47.4	99.16	70.77	35.13	88.01	58.14	39.03	98.02	79.03	68.94	75.82	40.47	52.08	29.83	69.2	34.2
Ba	486.57	773.6	526.23	593.66	472.57	410.76	503.56	498.91	446.89	537.41	272.23	486	397	411	269	291	510	550	540
Th	4.27	4.2	4.03	4.69	3.93	2.13	3.24	4.2	4.01	4.85	3.86	2.98	2	2.69	1.26	2.54	7.61	8.31	8.65
U	5.21	3.35	3.77	4.73	3.98	4.75	4.12	3.75	4.18	7.18	5.21	1.01	0.86	1.18	0.6	0.91	1.78	2.04	1.73
Nb	9.69	5.07	8.35	3.52	8.89	9.69	5.13	6.27	5.15	3.43	5.72	3.36	3.13	4.34	3.49	3.44	8.41	7.57	8.75
K	21,809	55,783	33,860	43,364	32,466	16,762	23,381	21,365	30,407	23,254	34,585	30,129	27,473	23,987	16,766	20,003	28,801	23,904	25,730
La	34.2	28.7	22.16	31.22	28.7	24.3	15.6	21.45	10.9	11.02	11.49	12.3	11.15	12.94	14.48	13.06	34.2	32.11	41.03
Ce	34.5	36.2	44.1	39.8	28.6	31.2	25.4	33.2	21.12	20.46	22.25	21.1	26.61	24.14	26.4	20.16	31.82	32.57	43.2
Pb	100	66.34	50.21	39.48	79.01	119.74	27.13	79.9	110.9	30.8	93.69	77.51	32.66	41.88	57.96	30.48	12.72	13.59	12.95
Pr	5.12	5.41	7.66	7.49	7.92	6.68	8.47	6.08	7.56	8.89	4.34	3.35	3.19	3.45	2.97	4.33	6.34	6.69	6.46
Sr	815.73	306.63	380.66	438.39	300.38	820.94	712.42	680.76	333.53	958.3	615.82	540.7	571.5	915.5	865.7	837	441	696	566
Nd	21.01	17.7	17.01	13.78	13.95	20.13	22.66	16.97	10.96	23.41	14.54	14.6–1	13.92	15.9	13.02	19.06	25.55	26.5	25.62
Zr	43.07	39.61	29.93	36.01	16.85	40.86	51.02	51.65	28.75	66.21	30.46	34.23	41.55	35.07	59.35	34.11	85.95	99.6	89.54
Sm	2.62	3.89	4.27	5.92	2.99	7.14	4.61	7.91	4.42	7.13	2.99	3.17	2.98	3.3	2.61	3.98	5.07	5.38	5.63
Eu	0.71	0.81	1.26	0.93	1.15	0.77	0.85	0.81	1.44	0.57	0.43	0.99	0.95	1.04	0.86	1.19	1.48	1.52	1.42
Ti	5,280	1,440	2,280	3,120	2,400	5,400	4,260	3,480	2,280	2,600	1,560	3,060	3,060	2,940	2,940	3,960	4,200	5,280	5,340
Dy	4.9	2.53	2.39	2.41	2.79	2.95	3.59	3.96	2.61	4.17	3.7	2.37	2.31	2.57	2.18	2.97	4.31	4.42	4.24
Y	18.07	4.53	11.1	12.55	8.55	17.23	13.34	13.57	11.32	28.73	5.2	12.13	11.91	13.19	11.27	15.1	21.99	21.27	21.72
Yb	2.55	0.87	1.17	1.86	1.18	2.32	1.65	1.81	1.37	1.75	0.94	1.29	1.25	1.45	1.3	1.57	2.28	2.24	2.26
Lu	0.4	0.34	0.37	0.43	0.39	0.3	0.15	0.32	0.38	0.27	0.27	0.2	0.29	0.22	0.2	0.24	0.26	0.24	0.35

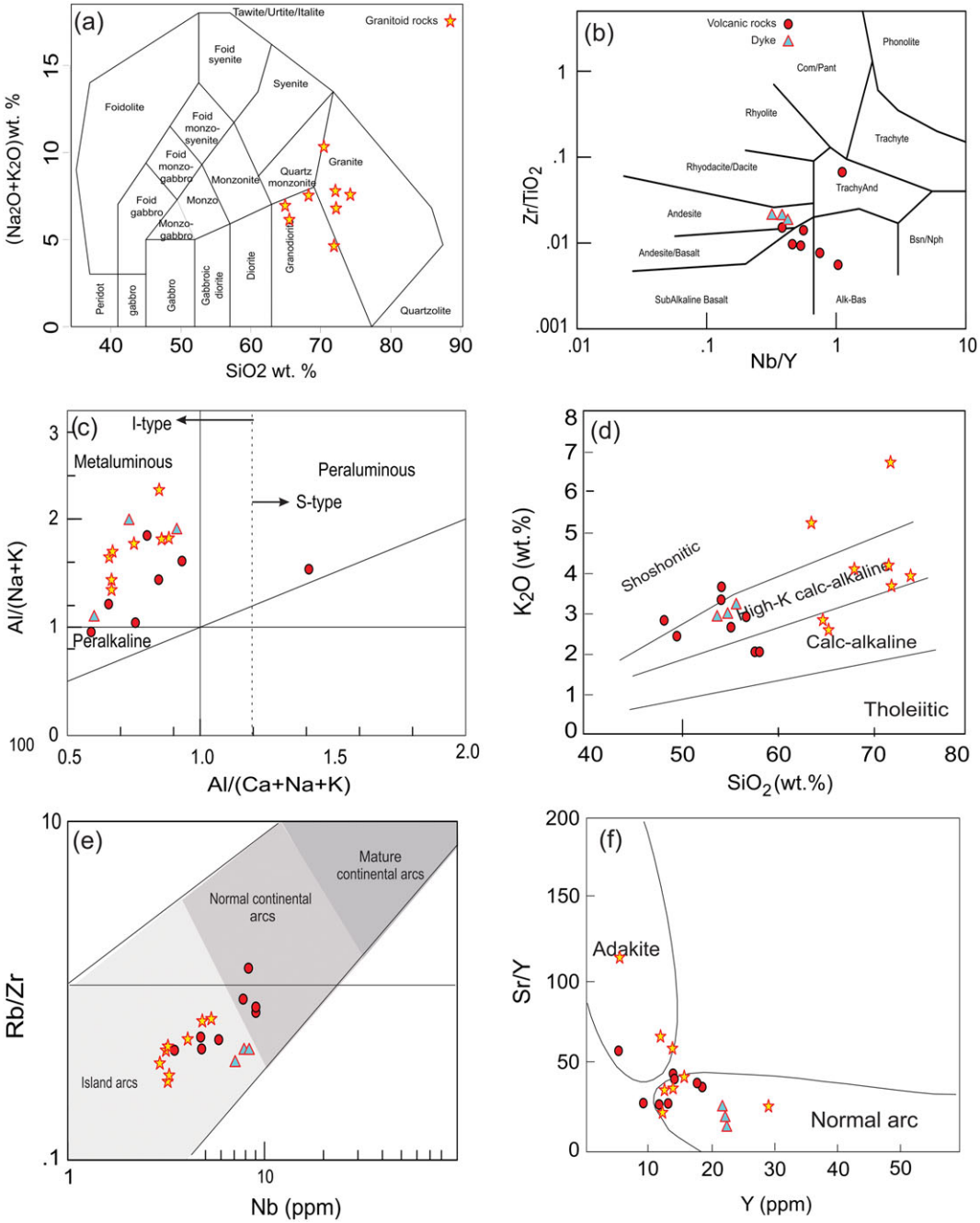

FIGURE 6 (a) $Na_2O + K_2O$ vs. SiO_2 classification diagram (Middlemost, 1994) of the Baghu intrusive rocks, with chemical variations ranging between granite, granodiorite, and diorite. (b) Nb/Y vs. Zr/TiO_2 (after Winchester & Floyd, 1977) to classify the volcanic Rocks of Baghu gold deposit. (c) A/NK vs. A/CNK diagram for the studied rocks. Field boundaries between I-type and S-type granitoids are from Chappell and White (1974), and peraluminous and metaluminous fields are from Shand (1943). ASI = molar $Al_2O_3/(Na_2O + K_2O + CaO)$. (d) SiO_2 vs. K_2O diagram (Peccerillo & Taylor, 1975). (e) Geochemical classification plots of the island-arc to Andean-arc intrusions in the Rb/Zr vs. Nb diagram (Brown et al., 1984). (f) Sr/Y vs. Y plot for samples from Baghu igneous rocks. Adakites and island-arc fields are adopted from Defant and Drummond (1990) [Colour figure can be viewed at wileyonlinelibrary.com]

5.2 | Zircon U–Pb data

The cathodoluminescence (CL) images and U–Pb age results are shown in Figures 8 and 9 and are given in Table 2 and 3.

The zircon grains from sample B41 (granodiorite; 10 spots), TRU5 (andesite; six spots), and TRU9 (dyke; five spots) were dated by ion probe technique. CL images show that the size of euhedral to subhedral zircon grains from granodiorite, andesite, and dykes ranges from 100 to 300 mm (Figure 8a), 100 to 300 mm (Figure 8b), and 100 to 250 mm (Figure 8c), respectively. Zircons from granodiorite have low to high U (74–2,033 ppm) and Th (59–1,451 ppm) concentrations, and Th/U ratios are >0.1 (0.6–1.1), while those from andesites are characterized by low to high U (114–1,074 ppm) and Th (92–1,132 ppm) concentrations, and Th/U ratios are >0.1 (0.4–1.05).

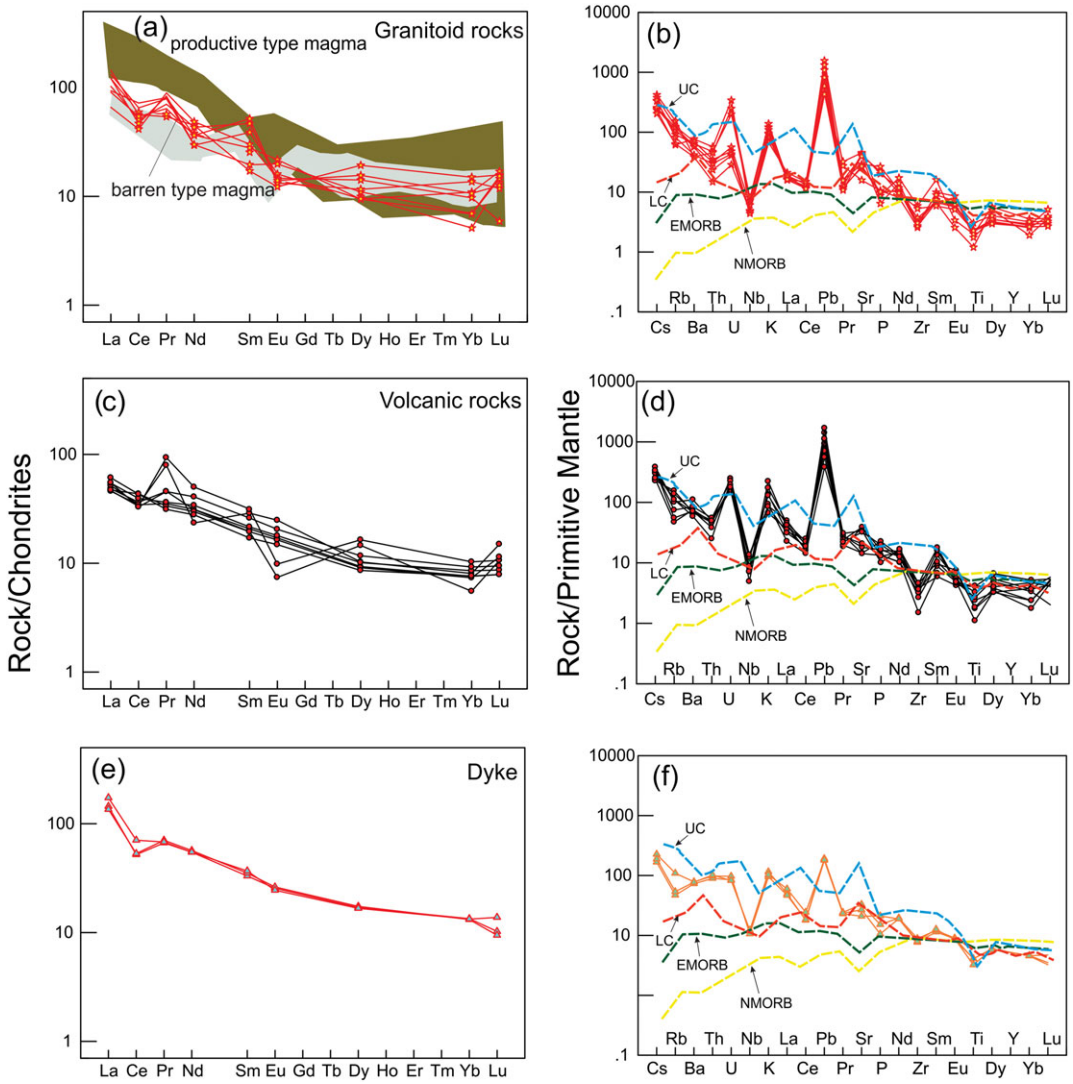

FIGURE 7 (a–f) Chondrite-normalized rare earth element (left) and N-MORB-normalized trace element spider patterns (right) for Baghu igneous rocks. Chondrite and N-MORB-normalized values are taken from Sun and McDonough (1989) [Colour figure can be viewed at wileyonlinelibrary.com]

Colour online, B&W in print

Similar to zircons of granodiorite and volcanic rocks, zircons from dykes have low to high U (114–1,074 ppm) and Th (92–1,132 ppm) concentrations, and Th/U ratios are >0.1 (0.4–1.05).

All these zircons from different lithologies show oscillatory zoning in CL images. The analyses for age calculations are concordant within analytical uncertainties, and all of them give a weighted mean age of 43.4 ± 1.3 Ma (MSWD = 0.008) (Figure 9a), 47.5 ± 2.4 Ma (mean square of the weighted deviates; York, 1967, 1969; MSWD = 0.21) (Figure 9b), and 38.0 ± 0.87 Ma (MSWD = 0.03) (Figure 9c) for granodiorite, andesite and dykes, respectively.

6 | DISCUSSION

6.1 | Petrogenesis and magma sources

Numerous processes have been proposed to describe the genesis of granitoids, including (i) partial melting of continental crust (Roberts & Clemens, 1993) or subducted oceanic crust (adakite; Defant & Drummond, 1990), (ii) fractional crystallization of basaltic or dioritic rocks (Macpherson, Dreher, & Thirlwall, 2006), (iii) magma mixing between basaltic and felsic rocks, and (iv) assimilation of crustal rocks (Davidson & Tepley, 1997).

The high K calc-alkaline granitoid rocks (43 Ma) from the Baghu gold deposit have similar trace element and REE patterns, $K_2O + Na_2O$ contents, and K_2O/Na_2O ratios. Older volcanic rocks (47 Ma) in this region display geochemical characteristics of mafic to intermediate igneous rocks. This indicates that the igneous rocks in the Baghu gold deposit could be directly formed from the same source. The chemical composition of the Baghu plutonic and volcanic rocks resembles the overall geochemical characteristic observed for this arc in north to north-east of Iran. They have silica content that ranges from ~48.5 to 58.5 wt.% and 63.9 to 72.3 wt.% for volcanic and granitoids rocks, respectively, with relatively similar ages, ruling out derivation from distinct magma sources. Metaluminous, high K calc-alkaline compositions, coupled with Rb–Nb + Y concentrations (Figure 10), point to derivation from subduction-related arc magmatism in a continental margin setting. The low Mg# (8 to 48) values and K enrichments

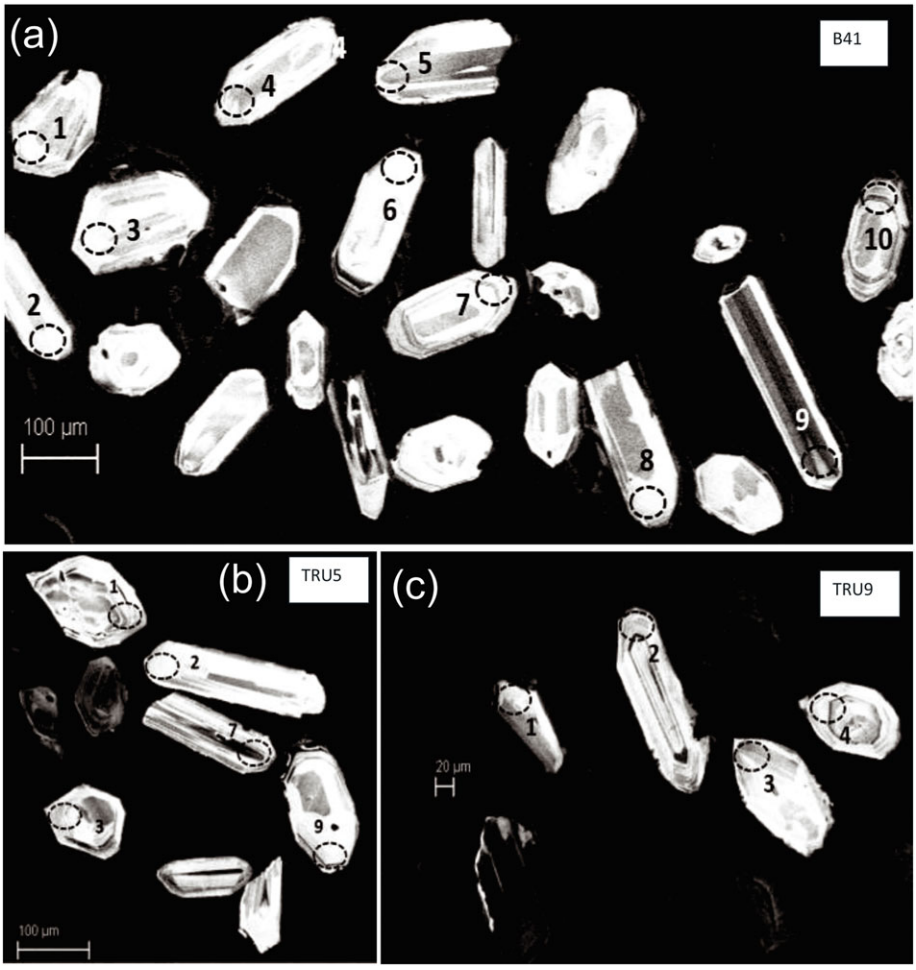

FIGURE 8 Cathodoluminescence image of zircon separate U–Pb for the Baghu gold deposit. (a) Andesite, (b) subvolcanic granodiorite, and (c) dykes [Colour figure can be viewed at wileyonlinelibrary.com]

clearly link these rocks to magmas that underwent a degree of magma differentiation and crustal contamination.

The strong similarity in the chondrite-normalized REE patterns (Figure 7) for the volcanic and plutonic samples suggests a common magma source and petrogenetic mechanism. LREE-enriched slopes without well-developed negative Eu anomalies evoke a magmatic source that fractionated important amounts of garnet; however, this may also reflect an elemental mixture of the asthenospheric mantle-derived basaltic magma with the crust. The involvement of crustal materials in the magma products is clearly observed by the multi-element diagrams, where the distinctive negative Nb and Ti anomalies, coupled with the enrichments in K and Pb, strongly support the role of asthenospheric mantle-derived basaltic magma with the crust.

It is believed that normal arc magmas are produced by partial melting of the mantle wedge that evolved to more felsic magmas by crystal fractionation or assimilation-crystal fractionation (Straub & Zellmer, 2012) and or magma mixing between two distinct mafic and felsic magmas. Due to lack of mafic micro-granular enclaves and petrographic textures such as acicular apatite, the resorption surfaces in plagioclase, sieve, and dusty textures, the role of magma mixing can be excluded on their genesis. Thus, a comparison of La/Sm against La (ppm) indicates that the Baghu igneous rocks have experienced partial melting rather than fractionation crystallization (Figure 10b). Moreover, LILEs and HFSEs have different geochemical behaviours in fluids and melts (Hawkesworth, Turner, Peate, McDermott, & Van Calsteren, 1997). LILEs, such as Rb, Ba, Sr, K, and U, are relatively mobile in fluids released from the subducted slab, whereas Th, LREEs, and HFSEs are mobilized by the melts (Class, Miller, Goldstein, & Langmuir, 2000; Elliott, Plank, Zindler, White, & Bourdon, 1997; Hawkesworth et al., 1997; Pearce & Peate, 1995). The clear enrichment of LILEs and LREEs, the depletion of HFSEs (Figure 7), and the low Ba/Th (70.5–213.5) and Th/Yb (18.5–48.8) ratios of the magmatic rocks (Figure 11a,b) indicate that a source was not significantly modified by previous slab-derived fluids (Elliott et al., 1997; Pearce & Peate, 1995). The Baghu gold igneous rocks have low Th/Nb and Th/Yb ratios (Figure 11a,b) that indicate that the source was not modified by slab-derived melts (Class et al., 2000; Johnson & Plank, 1999). The Baghu granitoid and volcanic rocks have similar Th/Nb and Th/Yb ratios to the crust and lower continental crust (LCC) (Figure 11a,b) and slightly higher than N-MORB, indicating the influence of partial melting of lower crust on Th/Nb and Th/Yb ratios of the Baghu igneous rocks, which is in agreement with trend of normalized trace elements on the N-MORB mantle-normalized (Sun & McDonough, 1989) multi-element diagram, enrichment in Rb, Ba, Th, U, and K and negative anomalies in Nb and Ti are similar to those from crust (Figure 7). These rocks have slightly similar Th/Nb and Th/Yb ratios to the average

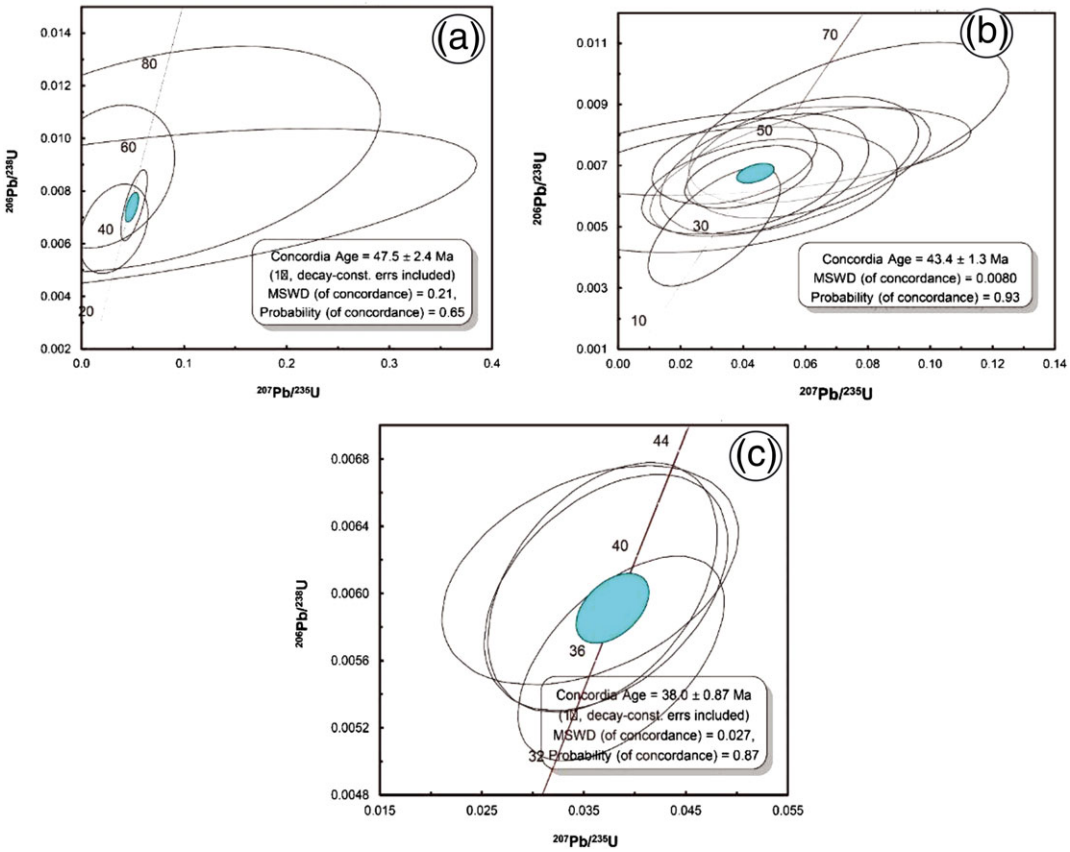

FIGURE 9 Zircon U–Pb ages for the andesite (a), subvolcanic granodiorite (b), and dykes (c) at the Baghu gold deposit. See Tables 2 and 3 [Colour figure can be viewed at wileyonlinelibrary.com]

TABLE 2 Zircon U–Pb dating results for magmatic rock from the Baghu gold deposit

Sample ID	UTM (WGS84)	Rock type	Age (Ma)	1 sigma age error (Ma)
B41	287181.00 E 3925933.00 N	Micro-granodiorite	43.4	1.3
TRU5	284757.77 E 3924273.23 N	Andesite	47.5	2.4
TRU9	287526.00 E 3926151.00 N	Diorite	38	0.87

global sediment from subduction zone settings (GLOSS), E-MORB, and N-MORB (Figure 11a,b), which supports the role of N-MORB (depleted mantle) source in their genesis (Dokuz, 2011; Hawkesworth et al., 1997; Oyarzun, Lillo, & Oyarzun, 2008). Rudnick and Gao (2003) estimated that the average $(La/Yb)_n$ of the lower continental crust is about 5.3, which is significantly more than that of the average MORB (~0.8; Sun & McDonough, 1989). The average $(La/Yb)_n$ of granitoids from Baghu is about 6.1, which is similar to average $(La/Yb)_n$ of the lower continental crust. It seems that partial melting of juvenile lower crust by melts originated from mantle may explain rare earth and trace element composition of igneous rocks from Baghu gold–copper deposits. However, it is clear from Figure 12 that granitoid rocks may be formed from garnet-amphibolite (30%) or eclogite whereas volcanic rock and dykes possibly are generated from garnet-amphibolite (3–10%) and amphibolite, respectively. However, the relatively high La/Nb (2.1–8.7) and low La/Ba (0.02–0.08) ratios, enrichment of LILE (e.g., Rb, Ba, Th, and K), and enrichment of LREEs and depletion of HFSE in the studied igneous rocks advocate partial melting of an enriched subcontinental lithospheric mantle. It is believed that Rb/Sr, Nb/La, and Nb/Ce are important tracers of mantle or crust source, since rocks derived from mantle have very low Rb/Sr ratios, 0.01–0.1 (Hofmann, 1988; Taylor and McLennan, 1985), which are lower than those of the lower continental crust (Rb/Sr = 0.12) and middle continental crust (Rb/Sr = 0.22) (Rudnick & Fountain, 1995; Wedepohl, 1995). The Rb/Sr ratios of the Baghu igneous rocks vary widely between 0.04 and 0.33, much higher than those of rocks derived from mantle. In addition, the contents of Nb/La and Nb/Ce in the mantle are about 1.01 and 0.39 (Sun & McDonough, 1989),

TABLE 3 Zircon U–Pb data by LA–ICP–MS for the andesite (B41), subvolcanic granodiorite (TRU5), and dioritic dykes (TRU9) at the Baghu gold deposit

Name	Age (Ma) $^{206}Pb/^{238}U$	Age (Ma) $^{206}Pb/^{238}U$ 1 *SE*	Age (Ma) $^{207}Pb/^{235}U$	Age (Ma) $^{207}Pb/^{235}U$ 1 *SE*	Age (Ma) $^{207}Pb/^{206}Pb$	Age (Ma) $^{207}Pb/^{206}Pb$ 1 *SE*	% Radiogenic ^{206}Pb	$^{207}Pb^*/^{235}U$	$^{207}Pb^*/^{235}U$ 1 *SE*	$^{206}Pb^*/^{238}U$	$^{206}Pb^*/^{238}U$ 1 *SE*	Correlation of concordia ellipses	$^{207}Pb^*/^{206}Pb^*$	$^{207}Pb^*/^{206}Pb^*$ 1 *SE*	U (ppm)	Th (ppm)	BA51 56 63 0.7	BA52 54.02 0.88	BA53 56.02 0.83
B41-7	32.13	5.09	30.71	8.53	−1	0.00955	99.33	0.0307	0.00865	0.005	0.000794	0.657	0.0446	0.00955	153	155	19.48	16.69	14.69
B41-5	39.92	5.39	32.84	22.7	−1	0.0258	92.87	0.0329	0.0231	0.00621	0.000841	0.316	0.0384	0.0258	137	109	0.12	0.14	0.11
B41-3	40.55	4.08	39.57	12.9	−1	0.0138	97.96	0.0397	0.0132	0.00631	0.000636	0.435	0.0457	0.0138	201	227	1.57	3.76	3.76
B41-10	42.55	2.68	41.54	8.14	−1	0.00826	98.28	0.0418	0.00835	0.00662	0.000418	0.447	0.0457	0.00826	195	131	6	7.59	6.95
B41-2	43.22	5.14	46.46	13.3	217.3	621	96.67	0.0468	0.0137	0.00673	0.000803	0.404	0.0505	0.0135	172	152	4.24	3.19	4.91
B41-6	43.66	5.53	54.51	17.7	561.9	607	97.77	0.0552	0.0184	0.0068	0.000863	0.586	0.0589	0.0164	2033	1451	3.47	2.88	3.18
B41-8	45.88	3.67	37.11	10.6	−1	0.0102	92.92	0.0372	0.0108	0.00714	0.000574	0.384	0.0378	0.0102	186	156	0.46	0.33	0.23
B41-4	46.66	5.2	58.39	14.5	570.4	509	97.4	0.0592	0.0152	0.00727	0.000813	0.41	0.0591	0.0138	74	59	5.56	8.36	6.36
B41-9	48.01	3.79	45.09	26.9	−1	0.0256	86.49	0.0454	0.0277	0.00748	0.000592	0.424	0.0441	0.0256	240	258	1.28	1.4	1.4
B41-1	53.89	6.9	72.8	19.8	748.8	495	100.6	0.0743	0.021	0.0084	0.00108	0.568	0.0642	0.015	183	152	99.51	99 24	99 24
																	1.32	1.79	1.49
TRU5-1	42.23	4.44	31.72	13.4	−1	0.0142	97	0.0317	0.0136	0.00657	0.000693	0.338	0.035	0.0142	809	566	29.83	69.2	34.2
TRU5-9	45.95	8.43	5.399	157	−1	0.157	36.6	0.00533	0.155	0.00715	0.00132	0.58	0.00541	0.157	147	104	510	550	540
TRU5-7	47.94	3.53	51.14	5.12	203.8	165	100.3	0.0517	0.0053	0.00746	0.000552	0.722	0.0502	0.00357	1074	1132	7.61	8.31	8.65
TRU5-3	54.92	7.08	24.88	26.9	−1	0.0225	87.96	0.0248	0.0271	0.00856	0.00111	0.26	0.021	0.0225	346	244	1.78	2.04	1.73
TRU5-2	59.08	11.2	69.41	85.6	441.5	2700	33.33	0.0708	0.0903	0.00921	0.00175	0.397	0.0557	0.0676	114	92	8.41	7.57	8.75
Not used in calculation																	28,801	23,904	25,730
TRU5-8	520.5	29	554.9	27.3	698.7	62.7	100.4	0.727	0.0465	0.0841	0.00487	0.888	0.0627	0.00185	208	90	34.2	32.11	41.03
																	31.82	32.57	43.2
TRU9-4	36.09	1.59	38.47	4.04	189.5	210	96.22	0.0386	0.00413	0.00562	0.000249	0.55	0.0499	0.00451	437	257	12.72	13.59	12.95
TRU9-2	38.61	1.84	37.06	4.76	−1	0.00534	99.12	0.0372	0.00487	0.00601	0.000287	0.422	0.0449	0.00534	242	158	6.34	6.69	6.46
TRU9-3	38.8	1.94	36.72	4.49	−1	0.005	98.55	0.0368	0.00458	0.00604	0.000303	0.421	0.0443	0.005	338	223	441	696	566
TRU9-1	39.27	1.7	35.53	5.81	−1	0.00655	95.26	0.0356	0.00593	0.00611	0.000266	0.387	0.0423	0.00655	265	142	25.55	26.5	25.62
Not used in calculation																	85.95	99.6	89.54
TRU9-6	564.1	28.9	568	24.8	583.6	53.7	99.98	0.75	0.0427	0.0915	0.00489	0.902	0.0595	0.00147	378	190	5.07	5.38	5.63

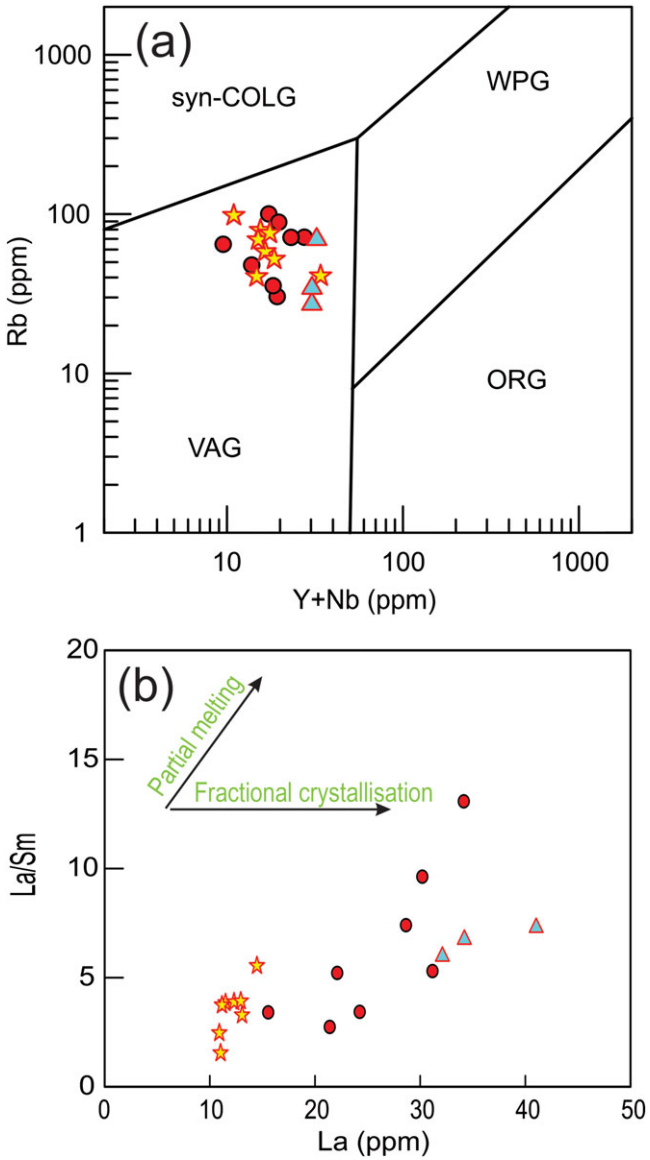

FIGURE 10 (a) Rb vs. Y + Nb (ppm) discrimination diagram of Pearce et al. (1984). (b) La/Sm vs. La (ppm) vs. (Treuil and Joron, 1975); the Baghu igneous rock plots in the field of I-type volcanic arc granite (VAG). VAG, volcanic arc granites (I-type); WPG, within-plate granites (A-type); ORG, ocean-ridge granites; syn-COLG, syncollisional granites (S-type) [Colour figure can be viewed at wileyonlinelibrary.com]

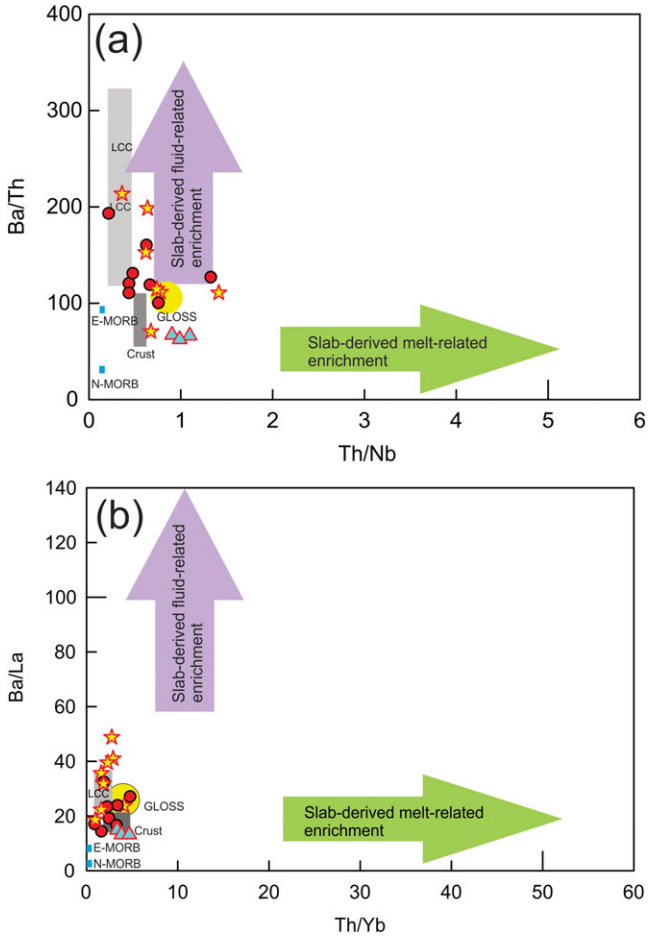

FIGURE 11 Th/Nb vs. Ba/Th diagram (a) (after Elliott et al., 1997) and Th/Yb vs. Ba/La diagram (b) (after Dokuz, 2011) for the studied intrusive and volcanic rocks (lower continental crust [LCC] and crust from Rudnick & Fountain, 1995; N-MORB and E-MORB from Sun & McDonough, 1989; GLOSS from Plank & Langmuir, 1988) [Colour figure can be viewed at wileyonlinelibrary.com]

respectively, while in the crust, they are about 0.46 and 0.23, respectively (Weaver & Tarney, 1984). The Nb/La and Nb/Ce ratios in the Baghu igneous rocks are from 0.17 to 0.47 and 0.18 to 0.31, respectively, different from those of rocks derived from the mantle, which indicate participation of lower crust in the source region. The lack of negative Eu anomalies (Figure 7) suggests that high levels of magmatic water, which suppressed plagioclase crystallization until late stages of fractionation, were prevalent (Keller, Schoene, Barboni, Samperton, & Husson, 2015). The absence of negative Eu anomalies can also be ascribed to the oxidizing conditions (Rollinson, 1993), such that Eu is present as Eu^{3+}, not Eu^{2+}. The enrichment of LREE and flat patterns of MREE to HREE (Figure 6a) can reflect amphibole fractionation from hydrous or enrichment of plagioclase. The profiles

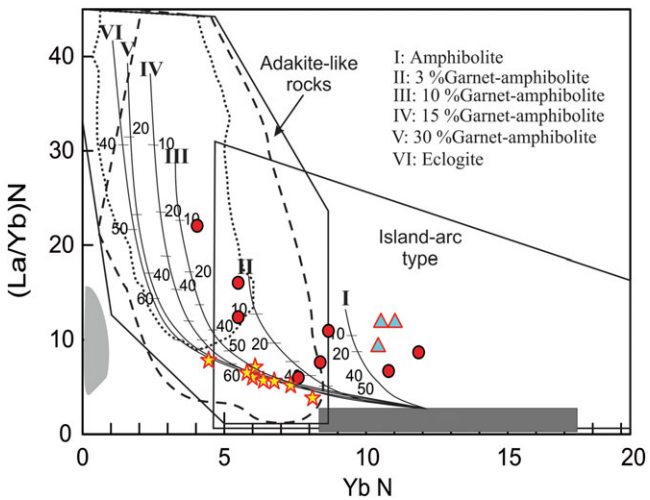

FIGURE 12 Diagram of batch-melting modelling of chondrite-normalized $[La/Yb]_n$ ratios vs. $[Yb]_n$ after Drummond et al. (1996) [Colour figure can be viewed at wileyonlinelibrary.com]

Colour online, B&W in print

Colour online, B&W in print

Colour online, B&W in print

of the REE and the unfractionated HREE (and Y) patterns (Figure 6b) suggest that the magmas were produced outside the garnet stability field, likely from an amphibole-bearing mantle source overlain by a relatively thin crust (Feigenson, Patino, & Carr, 1996). To explain the origin of the granitoid and volcanic rocks as porphyry copper deposits (PCDs) normal and adakite-likes, we applied a geochemical modelling (Drummond, Defant, & Kepezhinskas, 1996) based on $(La/Yb)_n$ vs. $(Yb)_n$ to show that many of the productive and barren porphyries can be generated by melting of the presumed garnet-amphibolite/eclogite sources (Rapp, Watson, & Miller, 1991; Tepper, Nelson, Bergantz, & Irving, 1993) and lack of plagioclase as a residual mineral. By using this modelling, it can be suggested that magmas were produced by partial melting of the lower continental crust in the presence of garnet. This model also indicates that 20–50% melting of a garnet-bearing amphibolite (30%) source can explain the geochemical composition of the Baghu igneous rock (Figure 12).

6.2 | Constraints on barren or productive magmatism in Baghu gold–copper deposit

The Baghu igneous rocks are I-type, subduction-related calc-alkaline igneous rocks with geochemical signatures indicative of being derived from the mixture of crust and mantle. They typically have variable K_2O (2.0–6.7 wt.%) and low Na_2O (0.3–4.9 wt.%) contents, similar to I-type granites with metaluminous signatures (Chappell & White, 2001). The P_2O_5 contents of the Baghu igneous rocks vary from 0.2% to 0.6% and decrease with increasing SiO_2 according to conventional classification schemes (Table 1), confirming that these rocks are I-type. Moreover, Rb/Sr ratios of up to 0.8 (<0.9) are similar to I-type granites (e.g., Wang, Xie, Hu, You, & Cao, 1993). The I-type granite signatures of the studied granodiorite are supported by the presence of hornblende and lack of aluminous primary minerals such as muscovite cordierite, tourmaline, andalusite, and garnet, with Rb/Sr ratios of up to 0.8 (<0.9; Wang et al., 1993). The Baghu granitoids and volcanic rocks are depleted in Nb–Ti and enriched in Ba, Th, Rb, U, Pb, and K, similar to arc-like rocks (with calc-alkaline affinity). However, syn- to post-collisional rocks are also characterized by HFSE depletions and LILE enrichments (Pearce, Harris, & Tindle, 1984), so these criteria are not definitive in all cases. N-MORB-normalized trace element patterns of productive-type samples are characterized by enrichment in Cs, Rb, Ba, Pb, and depletion in Nb, Ta, Th, Zr, Hf, and Ti. It has been suggested that the productive porphyries have distinct negative Nb, Ta, and Ti anomalies relative to barren-type granitoids (Asadi et al., 2014), suggesting that garnet was involved as a residual phase, at a pressure of >1.5 GPa (e.g., Xiong, Xia, Xu, Niu, & Xiao, 2006). The barren-type granitoid rocks show significant enrichment in HREE+Y (Figure 7a–f), which suggest that the sub-productive to barren porphyries are distinctly less fractionated ($[La/Yb]_n$ = 2.8–5.7) relative to productive types ($[La/Yb]_n$ = 12.5–39.6) (Karsli et al., 2011; Li et al., 2011; Richards, Spell, Rameh, Razique, & Fletcher, 2012). The granitoids from Baghu are enriched in Cs, Rb, Ba, and Pb and depleted in Nb, Ta, Th, Zr, Hf, and Ti, which implies that they have a similar trend with barren to sub-productive-type magmas.

On Rb vs. Y + Nb tectonic discrimination diagram, the Baghu granitoids and volcanic rocks plot in the VAG (volcanic arc granites) domain (Figure 10a); a similar setting is shown for the barren and sub-productive-type granitoids from UDMA in this diagram. On a Rb/Zr vs. Nb tectonic setting discrimination diagram, most Baghu lithologies plot in fields for island arc to continental settings (Figure 6e). It has been suggested that barren-type granites form in island arcs towards continental-arc, while those from productive-type rocks all form in the Andean-type arc setting. Therefore, it can be suggested that Baghu igneous rocks were originated from barren to sub-productive-type magmas.

The new U–Pb ages for the Baghu intrusive rocks reported here show that emplacement occurred at ca. 47–38 Ma. These ages are consistent within the range of major barren igneous activity in the UDMA including frontal and rear arcs.

In an Y vs. MnO diagram (Baldwin & Pearce, 1982), the Baghu samples plot in the sub-productive to barren igneous rocks (Figure 13a). Haschke and Pearce (2006) suggested that a high Y content in a barren magma may specify the participation of anhydrous phases during the early evolution of the magma and thus a lack of large mineralization associated with this magmatism. The relatively low Sr/Y (26–76) ratios of the Eocene Baghu igneous rocks are indicative of earlier to later island-arc magmatism, while a Sr/Y ratio of >56 for productive rocks implies garnet, hornblende, and clinopyroxene minerals in the source, leading to enrichment of LREE/HREE (Castillo, 2012). The La/Yb vs. SiO_2 diagram displays an

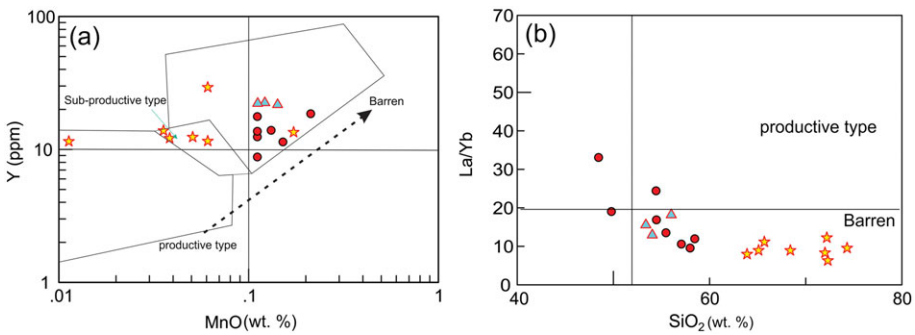

FIGURE 13 Diagrams of (a) MnO vs. Y (after Baldwin & Pearce, 1982) and (b) La/Yb vs. SiO_2 (after Richards et al., 2012) from the Baghu, showing barren (non-productive) to productive fields [Colour figure can be viewed at wileyonlinelibrary.com]

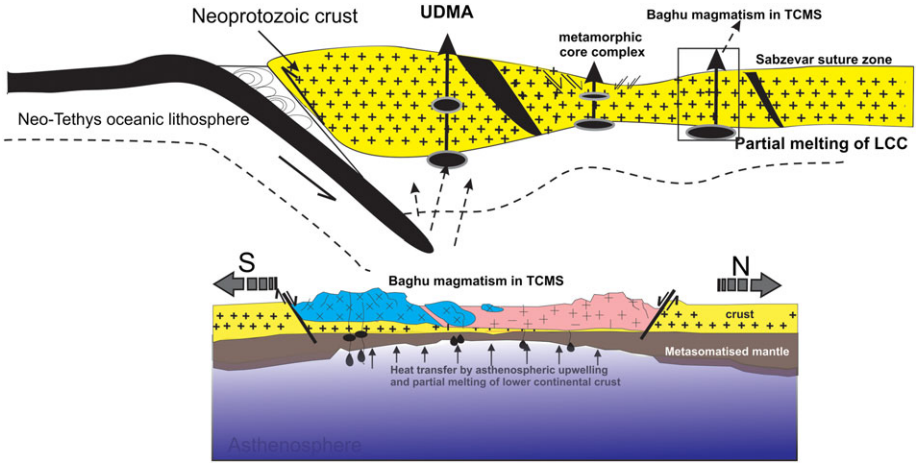

FIGURE 14 Schematic illustration showing the petrogenetic models for igneous rocks during the north-westward subduction of Neo-Tethys oceanic lithosphere (Verdel et al., 2011). Sub-productive normal arc magmatism: represented by the plutons of Baghu, formed by partial melting of juvenile mafic lower crust, which was interacted by storage of basaltic melts derived from the mantle [Colour figure can be viewed at wileyonlinelibrary.com]

almost low trend within the barren-type, implying earlier barren island-arc magmatism (Figure 13b).

6.3 | Geodynamic implications

The Eocene–Oligocene magmatic events in Iran represents magmatic pulses (Pang et al., 2013; Verdel et al., 2011), during a ~20–25 m.yr. time period (Chiu et al., 2013; Pang et al., 2013; Sepidbar, Mirnejad, Ma, & Shafaiim Moghadam, 2018), with an Andean-type belt of intrusive and extrusive rocks in the UDMA in frontal-arc and rear-arc (outer arc) regions. Break-off of the subducted continent–ocean transitional lithosphere beneath the Zagros Mountains (e.g., Molinaro et al., 2005) and/or lithospheric thickening with partial delamination to the north-east of the Zagros (e.g., Hatzfeld & Molnar, 2010) are suggested to have caused these magmatic pulses throughout Iran. During Late Cretaceous–Early Oligocene time, continuous convergence between Arabia and Iran led to the closure of the southern Neotethyan basin, emplacing the Late Cretaceous Zagros Iranian ophiolites during the transition from a compressional to an extensional convergent plate margin (Agard et al., 2011; Rossetti et al., 2014). In Iran, this extension, following the closure of the southern Neotethyan basin, was followed by opening of the rear arc during middle Eocene–Early Oligocene time in the north to north-east of Iran. Middle Eocene–Early Oligocene extension and lithospheric thinning, which are confirmed by ENE-striking strike–slip fault systems, might have been accompanied by decompression melting of upwelling hydrous asthenosphere (Verdel et al., 2011, 2007). Generally, such magmatic pulses are common in extensional settings above subduction zones and/or in post-collisional settings. The new geochemical data from this study emphasize that the Baghu igneous rocks are connected to the pooling of mafic magmas in the continental crust in the north of Iran, producing thermal anomalies and reworking of the crust (Figure 14). The reconstructed structural and petrologic scenario presented here can be integrated into a coherent tectonic/geodynamic framework that places the TCMS within the rear arc during Tertiary Arabia–Eurasia convergence.

7 | CONCLUSIONS

1. The results of zircon U–Pb age show that the barren to sub-productive granitoids, volcanic rocks, and dykes at Baghu formed in the Middle Eocene.
2. Major and trace element results show that the granitoids have calc-alkaline normal arc signatures with a depletion in Nb and Ti and enrichment in LREEs and LILEs; the relatively flat patterns for REEs confirm that they are related to barren to sub-productive systems.
3. A comparison of La/Sm against La (ppm), similar Th/Nb and Th/Yb, and average $(La/Yb)_n$ ratios to the crust and lower continental crust (LCC) suggests that the magmatism in the Baghu was likely associated with partial melting of juvenile lower crust, induced by north-westward subduction of the Neo-Tethys oceanic lithosphere in an extensional setting.
4. The geochemical results show that the mantle source was not likely modified by subduction of the Neo-Tethyan oceanic slab fluid and melt components beneath the central Iranian microcontinent between the early Eocene to the late Eocene.

ACKNOWLEDGEMENTS

The authors would like to thank the University of Tehran for various supports. The U–Pb data acquisition at UCLA was supported by the Caltech Tectonics Observatory under the auspices of Gordon and Betty Moore Foundation. The ion microprobe facility at UCLA is partly supported by a grant from the Instrumentation and Facilities Program, Division of Earth Sciences, National Science Foundation. D. L. is supported by a NSERC Discovery grant. We would like to thank Professor Ian D. Somerville for editorial handling of the paper, as well as

Professor Xue-Ming Yang and one anonymous reviewer for their constructive comments.

ORCID

Shojaeddin Niroomand https://orcid.org/0000-0001-8349-2896
Hassan Mirnejad https://orcid.org/0000-0001-9776-3570

REFERENCES

Agard, P., Omrani, J., Jolivet, L., Whitechurch, H., Vrielynck, B., Spakman, W., … Wortel, R. (2011). Zagros orogeny: A subduction-dominated process. *Geological Magazine*, *148*, 692–725. https://doi.org/10.1017/S001675681100046X

Aghazadeh, M., Hou, Z., Badrzadeh, Z., & Zhou, L. (2015). Temporal-spatial distribution and tectonic setting of porphyry copper deposits in Iran: constraints from zircon U-Pb and molybdenite Re-Os geochronology. *Ore geology reviews*, *70*, 385–406.

Asadi, S., & Moore, F. (2017). Fluid evolution in H_2O–CO_2–NaCl system and metallogenic analysis of the Surian metamorphic complex, Bavanat Cu deposit, Southwest Iran. *Mineralogy and Petrology*, *111*, 145–161. https://doi.org/10.1007/s00710-016-0457-z

Asadi, S., Moore, F., & Zarasvandi, A. (2014). Discriminating productive and barren porphyry copper deposits in the southeastern part of the central Iranian volcano-plutonic belt, Kerman region, Iran: A review. *Earth-Science Reviews*, *138*, 25–46. https://doi.org/10.1016/j.earscirev.2014.08.001

Asiabanha, A., Bardintzeff, J. M., Kananian, A., & Rahimi, G. (2012). Post-Eocene volcanics of the Abazar district, Qazvin, Iran: Mineralogical and geochemical evidence for a complex magmatic evolution. *Journal of Asian Earth Sciences*, *45*, 79–94. https://doi.org/10.1016/j.jseaes.2011.09.020

Baldwin, J. A., & Pearce, J. A. (1982). Discrimination of productive and non-productive porphyritic intrusions in the Chilean Andes. *Economic Geology*, *77*, 664–674. https://doi.org/10.2113/gsecongeo.77.3.664

Baumann, A., Spies, O., & Lensch, G. (1983). Strontium isotopic composition of post-ophiolitic Tertiary volcanic between Kashmar, Sabzevar and Quchan, NE Iran. *Geoogyl Mineral Survey Iran*, *51*, 267–275.

Berberian, M., & King, G. C. P. (1981). Towards a paleogeography and tectonic evolution of Iran. *Canadian Journal of Earth Sciences*, *18*, 210–265. https://doi.org/10.1139/e81-019

Brown, G. C., Thorpe, R., & Webb, P. C. (1984). The geochemical characteristics of granitoids in contrasting arcs and comments on magma sources. *Journal of Geological Society*, *141*, 413–426. https://doi.org/10.1144/gsjgs.141.3.0413

Castillo, P. R. (2012). Adakite petrogenesis. *Lithos*, *135*, 304–316.

Castro, A., Aghazadeh, M., Badrzadeh, Z., & Chichorro, M. (2013). Late Eocene–Oligocene post-collisional monzonitic intrusions from the Alborz magmatic belt, NW Iran. An example of monzonite magma generation from a metasomatized mantle source. *Lithos*, *180*, 109–127.

Chappell, B. W., & White, A. J. R. (1974). Two contrasting granite types. *Pacific Geology*, *8*, 173–174.

Chappell, B. W., & White, A. J. R. (2001). Two contrasting granite types: 25 years later. *Australian Journal of Earth Sciences*, *48*, 489–499. https://doi.org/10.1046/j.1440-0952.2001.00882.x

Chiu, H.-Y., Chung, S.-L., Zarrinkoub, M. H., Mohammadi, S. S., Khatib, M. M., & Iizuka, Y. (2013). Zircon U–Pb age constraints from Iran on the magmatic evolution related to Neotethyan subduction and Zagros orogeny. *Lithos*, *162–163*, 70–87.

Class, C., Miller, D. M., Goldstein, S. L., & Langmuir, C. H. (2000). Distinguishing melt and fluid subduction components in Umnak Volcanics, Aleutian Arc. *Geochemistry, Geophysics, Geosystems*. https://doi.org/10.1029/1999GC000010 (G3 1:1004)

Compston, W., Williams, I. S., & Meyer, C. (1984). U–Pb geochronology of zircons from Lunar Breccia 73217 using a sensitive, high mass resolution ion microprobe. *Journal of Geophysical Research*, *89*, 8525–8534.

Davidson, J. P., & Tepley, F. J. I. (1997). Recharge in volcanic systems; evidence from isotope profiles of phenocrysts. *Science*, *275*, 826–829. https://doi.org/10.1126/science.275.5301.826

Defant, M. J., & Drummond, M. S. (1990). Derivation of some modern arc magmas by melting of young subducted lithosphere. *Nature*, *347*, 662–665. https://doi.org/10.1038/347662a0

Dilek, Y., Imamverdiyev, N., & Altunkaynak, S. (2010). Geochemistry and tectonics of Cenozoic volcanism in the Lesser Caucasus (Azerbaijan) and the peri-Arabian region: Collision-induced mantle dynamics and its magmatic fingerprint. *International Geology Review*, *52*, 536–578. https://doi.org/10.1080/00206810903360422

Dokuz, A. (2011). A slab detachment and delamination model for the generation of Carboniferous high-potassium I-type magmatism in the Eastern Pontides, NE Turkey: The Kossel composite pluton. *Gondwana Research*, *19*, 926–944. https://doi.org/10.1016/j.gr.2010.09.006

Drummond, M. S., Defant, M. J., & Kepezhinskas, P. K. (1996). Petrogenesis of slab-derived trondhjemite–tonalite–dacite/adakite magmas. *Transactions of the Royal Society of Edinburgh: Earth Sciences*, *87*, 205–215. https://doi.org/10.1017/S0263593300006611

Elliott, T., Plank, T., Zindler, A., White, W., & Bourdon, B. (1997). Element transport from slab to volcanic front at the Mariana arc. *Journal of Geophysical Research*, *102*, 14991–15019. https://doi.org/10.1029/97JB00788

Fard, M., Rastad, E., & Ghaderi, M. (2006). Epithermal gold and base metal mineralization at Gandy, north of Central Iran and the role of rhyolitic intrusions. *Journal of Science Islamic Republic of Iran*, *17*, 327–335.

Feigenson, M. D., Patino, L. C., & Cart, M. J. (1996). Constraints on partial melting imposed by rare earth element variations in Mauna Kea basalts. *Journal of Geophysics*, *Res*. *101*, 11815–11829.

Haschke, M. & Pearce, J. A. (2006). Lithochemical exploration tools revisited: MnO and REE. GSA Abstracts with Programs, Speciality Meeting, Mendoza, Argentina, 2, 116.

Hatzfeld, D., & Molnar, P. (2010). Comparisons of the kinematics and deep structures of the Zagros and Himalaya and of the Iranian and Tibetan plateaus and geodynamic implications. *Rev. Geophys.*, *48*, RG2005. https://doi.org/10.1029/2009RG000304"10.1029/2009RG00030

Hawkesworth, C., Turner, S., Peate, D., McDermott, F., & Van Calsteren, P. (1997). Elemental U and Th variations in island arc rocks: Implications for U-series isotopes. *Chemical Geology*, *139*, 207–221. https://doi.org/10.1016/S0009-2541(97)00036-3

Hofmann, A. W. (1988). Chemical differentiation of the Earth: the relationship between mantle, continental crust, and oceanic crust. *Earth and Planetary Science Letters*, *90*(3), 297–314.

Houshmandzadeh, A. R., Alavi Naini, M., & Haghipour, A. A. (1978). Evolution of geological phenomenon in Torud area. *Geological Survey of Iran Report*, *H5*, 136. (in Persian with English abstract)

Johnson, M. C., & Plank, T. (1999). Dehydration and melting experiments constrain the fate of subducted sediments. *Geochemistry, Geophysics, Geosystem.*, *1*, 1007. https://doi.org/10.1029/1999GC000014

Karsli, O., Ketenci, M., Uysal, I., Dokuz, A., Aydin, F., Chen, B., Kandemir, R. & Wijbrans, J. (2011). Adakite-like granitoid porphyries in the Eastern Pontides, NE Turkey: potential parental melts and geodynamic implications. *Lithos*, *127*, 354–372.

Keller, C. B., Schoene, B., Barboni, M., Samperton, K. M., & Husson, J. M. (2015). Volcanic-plutonic parity and the differentiation of the continental crust. *Nature*, *523*, 301–307.

Li, J. X., Qin, K. Z., Li, G. M., Xiao, B., Chen, L., & Zhao, J. X. (2011). Post-collisional ore-bearing adakitic porphyries from Gangdese porphyry copper belt, southern Tibet: Melting of thickened juvenile arc lower crust. *Lithos*, *126*, 265–277. https://doi.org/10.1016/j.lithos.2011.07.018

Macpherson, C. G., Dreher, S. T., & Thirlwall, M. F. (2006). Adakites without slab melting: High pressure differentiation of island arc magma, Mindanao, the Philippines. *Earth and Planetary Science Letters*, *243*, 581–593. https://doi.org/10.1016/j.epsl.2005.12.034

Middlemost, E. A. K. (1994). Naming materials in the magma/igneous rock system. *Earth-Science Reviews*, *37*, 215–224. https://doi.org/10.1016/0012-8252(94)90029-9

Moghadam, H. S., & Stern, R. J. (2014). Ophiolites of Iran: Keys to understanding the tectonic evolution of SW Asia:(I) Paleozoic ophiolites. *Journal of Asian Earth Sciences*, *91*, 19–38.

Moradi, S. (2010). *Investigation of gold mineralization in the Baghu Area, Southeast of Damghan*. Master Dissertation. Damghan University, 1–224.

Niroomand, S., Hassanzadeh, J., Tajeddin, H. A., & Asadi, S. (2018). Hydrothermal evolution and isotope studies of the Baghu intrusion-related gold deposit, Semnan province, north-central Iran. *Ore Geology Reviews*, *95*, 1028–1048. https://doi.org/10.1016/j.oregeorev.2018.01.015

Oyarzun, R., Lillo, J., & Oyarzun, J. (2008). No water, no cyanobacteria–no calc-alkaline magmas: Progressive oxidation of the early oceans may have contributed to modernize island-arc magmatism. *International Geology Review*, *50*, 885–894. https://doi.org/10.2747/0020-6814.50.10.885

Pang, K. N., Chung, S. L., Zarrinkoub, M. H., Khatib, M. M., Mohammadi, S. S., Chiu, H. Y., … Lo, C. H. (2013). Eocene–Oligocene post-collisional magmatism in the Lut–Sistan region, eastern Iran: Magma genesis and tectonic implications. *Lithos*, *180*, 234–251.

Paces, J. B., & Miller, J. D. Jr (1993). Precise U-Pb ages of Duluth complex and related mafic intrusions, northeastern Minnesota: Geochronological insights to physical, petrogenetic, paleomagnetic, and tectonomagmatic processes associated with the 1.1 Ga midcontinent rift system. *Journal of Geophysical Research: Solid Earth*, *98*(B8), 13997–14013.

Pearce, J. A., Harris, N. B. W., & Tindle, A. G. (1984). Trace element discrimination diagrams for the tectonic interpretation of granitic rocks. *Jouranl of Petrology*, *25*, 956–998. https://doi.org/10.1093/petrology/25.4.956

Pearce, J. A., & Peate, D. W. (1995). Tectonic implications of the composition of volcanic arc magmas. *Annual Review of Earth and Planetary Sciences*, *23*, 251–285. https://doi.org/10.1146/annurev.ea.23.050195.001343

Peccerillo, A., & Taylor, S. R. (1975). Geochemistry of Upper Cretaceous volcanic rocks from the Pontic Chain, northern Turkey. *Bulletin of Volcanology*, *39*, 1–13.

Plank, T., & Langmuir, C. H. (1988). The chemical composition of subducting sediment and its consequences for the crust and mantle. *Chemical Geology*, *145*, 325–394.

Qi, L., Hu, J., & Gregoire, D. (2000). Determination of trace elements in granites by inductively coupled plasma-mass spectrometry. *Talanta*, *51*, 507–513.

Quidelleur, X., Grove, M., Lovera, O. M., Harrison, T. M., Yin, A., & Ryerson, F. J. (1997). Thermal evolution and slip history of the Renbu-Zedong thrust, southeastern Tibet. *Journal of Geophysical Research*, *102*, 2659–2679. https://doi.org/10.1029/96JD02483

Rapp, R. P., Watson, B. E., & Miller, C. F. (1991). Partial melting of amphibolite/eclogite and the origin of Archean trondhjemites and tonalities. *Precambrian Research*, *51*, 1–25. https://doi.org/10.1016/0301-9268(91)90092-O

Rashidnejad Omran, N. (1992). *The study of magmatic evolution in the Baghu area and relation with gold mineralization, SE Damghan*. (M.Sc. thesis) University of Tarbiat Moalem, Tehran, Iran, 324 pp.

Rastad, E., Fard, M., Rashidnejad-Omran, N. & Ghaderi, M. (1999). Mineralization and potential of gold in Torud-Chah Shirin volcano-plutonic complex (south Damghan) [abs.]. Geol. Soc. Iran, 214–215.

Richards, J. P., Spell, T., Rameh, E., Razique, A., & Fletcher, T. (2012). High Sr/Y magmas reflect arc maturity, high magmatic water content, and porphyry Cu ± Mo ± Au potential examples from the Tethyan arcs of Central and Eastern Iran and Western Pakistan. *Economic Geology*, *107*, 295–332. https://doi.org/10.2113/econgeo.107.2.295

Roberts, M. P., & Clemens, J. D. (1993). Origin of high-potassium, calc-alkaline, I-type granitoids. *Geology*, *21*, 825–828. https://doi.org/10.1130/0091-7613(1993)021<0825:OOHPTA>2.3.CO;2

Rollinson, H. U. (1993). *Using Geochemical Data: Evaluation, Presentation, Interpretation*. London, UK: Longman Scientific and Technical.

Rossetti, F., Nasrabady, M., Theye, T., Gerdes, A., Monie, P., & Lucci, F.& Vignaroli, G. (2014). Adakite differentiation and emplacement in a subduction channel: The late Paleocene Sabzevar magmatism (NE Iran). *Geological Society of America Bulletin*, *126*, 317–343. https://doi.org/10.1130/B30913.1

Rudnick, R. L., & Fountain, D. M. (1995). Nature and composition of the continental crust—A lower crustal perspective. *Reviews in Geophysics*, *33*, 267–309. https://doi.org/10.1029/95RG01302

Rudnick, R. L., & Gao, S. (2003). Composition of the continental crust. In D. H. Heinrich, & K. K. Turekian (Eds.), *Treatise on geochemistry* (pp. 1–64). Oxford: Pergamon. https://doi.org/10.1016/B0-08-043751-6/03016-4

Sanudo-Wilhelmy, S. A., & Flegal, A. R. (1994). Temporal variations in lead concentrations and isotopic composition in the Southern California. *Geochimica et Cosmochimica Acta*, *58*, 3315–3320. https://doi.org/10.1016/0016-7037(94)90060-4

Schmitt, A. K., Grove, M., Harrison, T. M., Lovera, O., Hulen, J. B., & Walters, M. (2003). The Geysers-Cobb mountain magma system California (part 1): U–Pb zircon ages of volcanic rocks conditions of zircon crystallization and magma residence times. *Geochimica et Cosmochimica Acta*, *67*, 3423–3442. https://doi.org/10.1016/S0016-7037(03)00140-6

Sepidbar, F., Mirnejad, H., Ma, C., & Shafaiim Moghadam, H. (2018). Identification of Eocene–Oligocene magmatic pulses associated with flare-up in east Iran: Timing and sources. *Gondwana Research*, *57*, 141–156. https://doi.org/10.1016/j.gr.2018.01.008

Shamanian, G. H., Hedenquist, J. W., Hattor, H., & Hassanzadeh, J. (2004). The Gandy and Abolhassani epithermal prospects in the Alborz magmatic Arc, Semnan province, northern Iran. *Economic Geology*, *99*, 691–712. https://doi.org/10.2113/gsecongeo.99.4.691

Shand, S. J. (1943). *The eruptive rocks: 2nd edition*. (pp. 444). New York: John Wiley.

Shand, S. J. (1974). *Eruptive rocks: Their genesis, composition classification, and their relation to ore-deposits (3rd edition)*. (pp. 488). New York: John Wiley and Sons.

Shaykhi, H. (2013). *Geology, alteration and gold genesis in Baghu deposit*. Master Dissertation. Damghan University, 187.

Stacey, J. C., & Kramers, J. D. (1975). Approximation of terrestrial lead isotope evolution by a two-stage model. *Earth and Planetary Science Letters*, *26*, 207–221. https://doi.org/10.1016/0012-821X(75)90088-6

Straub, S. M., & Zellmer, G. F. (2012). Volcanic arcs as archives of plate tectonic change. *Gondwana Reseach*, *21*, 495–516. https://doi.org/10.1016/j.gr.2011.10.006

Sun, S., & McDonough, W. F. (1989). Chemical and isotopic systematics of oceanic basalts: Implications for mantle composition and processes. *Geological Society*, *42*, 313–345. https://doi.org/10.1144/GSL.SP.1989.042.01.19

Taghipour, B., & Mackizadeh, M. A. (2014). The origin of the tourmaline-turquoise association hosted in hydrothermally altered rocks of the Kuh-Zar Cu-Au-turquoise deposit, Damghan, Iran. *Neues Jahrbuch für Geologie und Paläontologie-Abhandlungen*, *272*(1), 61–77.

Taylor, S. R., & McLennan, S. M. (1985). *The continental crust: its composition and evolution*. (pp. 312). Carlton: Blackwell Scientific Publication.

Tepper, J. H., Nelson, B. K., Bergantz, G. W., & Irving, A. J. (1993). Petrology of the Chilliwack batholite, north Cascades, Washington: Generation of calc-alkaline granitoids by melting of mafic lower crust with variable water fugacity. *Contributions to Mineralogy and Petrology*, *113*, 333–351. https://doi.org/10.1007/BF00286926

Treuil, M., & JoRoN, J.- L. (1975). Utilisation des elements hygromagmatophiles pour la simplification de la modelisation quantitative des processus magma-tiques. *Soc. Ital. Miner. Petrol., XXXI*, 125–174.

Verdel, C., Wernicke, B. P., Hassanzadeh, J., & Guest, B. (2011). A Paleogene extensional arc flare-up in Iran. *Tectonics*, *30*. https://doi.org/10.1029/2010TC002809

Verdel, C., Wernicke, B. P., Ramezani, J., Hassanzadeh, J., Renne, P. R., & Spell, T. L. (2007). Geology and thermochronology of Tertiary Cordilleran-style metamorphic core complexes in the Saghand region of central Iran. *Geological Society of America Bulletin*, *119*, 961–977. https://doi.org/10.1130/B26102.1

Wang, D. R., Xie, Y. M., Hu, Y. J., You, X. X., & Cao, J. X. (1993). Geology of Guogailiang area (Map G-48-1-A). Panxi Geological Team, Geology and Mineral Resources Bureau, Sichuan Province, 1:50000.

Weaver, B. L., & Tarney, J. (1984). Estimating the composition of the continental crust: an empirical approach. *Nature*, *310*, 575–577. https://doi.org/10.2138/am.2010.3371

Whitney, D. L., & Evans, B. W. (2010). Abbreviations for names of rock-forming minerals. *American Mineralogist*, *95*, 185–187.

Winchester, J. A., & Floyd, P. A. (1977). Geochemical discrimination of different magma series and their differentiation products using immobile elements. *Chemical Geology*, *20*, 325–343. https://doi.org/10.1016/0009-2541(77)90057-2

Xiong, X. L., Xia, B., Xu, J. F., Niu, H. C., & Xiao, W. S. (2006). Na depletion in modern adakites via melt/rock reaction within the sub-arc mantle. *Chemical Geology*, *229*, 273–292. https://doi.org/10.1016/j.chemgeo.2005.11.008

York, D. (1967). The best isochron. *Earth and Planetary Science Letters*, *2*, 479–482. https://doi.org/10.1016/0012-821X(67)90193-8

York, D. (1969). Least squares fitting of a straight line with correlated errors. *Earth and Planetary Science Letters*, *5*, 320–324.

Zanchi, A., Zanchetta, S., Berra, F., Mattei, M., Garzanti, E., Molyneux, S., … Sabouri, J. (2009). *The Eo-Cimmerian (Late? Triassic) orogeny in North Iran* (Vol. 312) (pp. 31–55)Geological Society London Special Publications. https://doi.org/10.1144/SP312.3

How to cite this article: Niroomand S, Lentz DR, Sepidbar F, Tajeddin HA, Hassanzadeh J, Mirnejad H. Geochemical characteristics of igneous rocks associated with Baghu gold deposit in the Neotethyan Torud-Chah Shirin segment, Northern Iran. *Geological Journal*. 2018;1–18. https://doi.org/10.1002/gj.3397